AD-A171 264 LOW-COST ALLOY PERMANENT MAGNET MATERIALS(U) GENERAL ELECTRIC CORPORATE RESEARCH AND DEVELOPMENT SCHENECTADY NY J D LIVINGSTON JUL 86 86SRD020 N00014-84-C-0296 1/1

UNCLASSIFIED F/G 11/6 NL

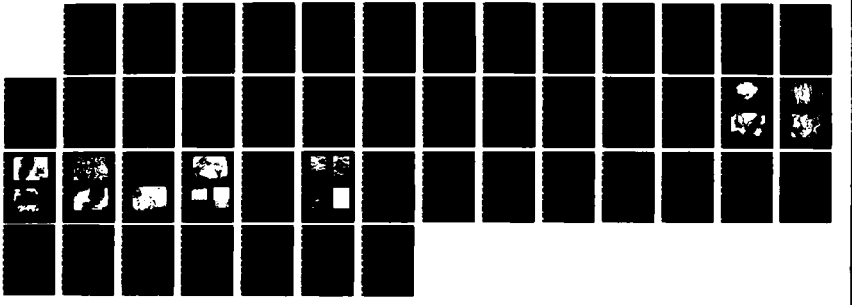

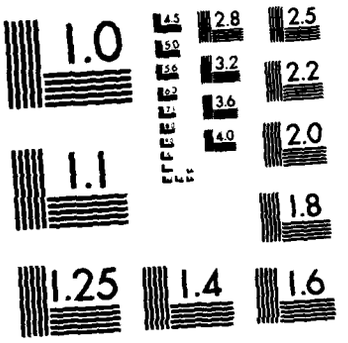

(12

AD-A171 264

LOW-COST ALLOY PERMANENT MAGNET MATERIALS

Final Report

Contract No. N00014-84-C-0296

Prepared for

Department of the Navy
800 North Quincy St.
Office of Naval Research
Arlington, Virginia 22217

Prepared by

Alloy Properties Branch
Materials Laboratory
Corporate Research and Development
P.O. Box 8
General Electric Company
Schenectady, New York 12301

July 1986

86SRD020

8a. NAME OF FUNDING/SPONSORING ORGANIZATION Department of the Navy Office of Naval Research	8b. OFFICE SYMBOL (If applicable)	9. PROCUREMENT INSTRUMENT IDENTIFICATION NUMBER N00014-84-C-0296			
8c. ADDRESS (City, State and ZIP Code) 800 North Quincy St. Arlington, Virginia 22217		10. SOURCE OF FUNDING NOS.			
		PROGRAM ELEMENT NO.	PROJECT NO.	TASK NO.	WORK UNIT NO.
11. TITLE (Include Security Classification) Low-Cost Alloy Permanent Magnet Materials (Unclassified)					
12. PERSONAL AUTHOR(S) J.D. Livingston					
13a. TYPE OF REPORT Final Report	13b. TIME COVERED FROM 84 May TO 86 May	14. DATE OF REPORT (Yr., Mo., Day) 86 July		15. PAGE COUNT 41	
16. SUPPLEMENTARY NOTATION					

17 COSATI CODES			18. SUBJECT TERMS (Continue on reverse if necessary and identify by block number)
FIELD	GROUP	SUB. GR.	

TABLE OF CONTENTS

LIST OF ILLUSTRATIONS

LIST OF ILLUSTRATIONS (Cont'd)

Section 1

BACKGROUND AND SUMMARY

For the past three years, worldwide attention in the area of permanent magnets has been focused on Fe-Nd-B and related materials. The late J.J. Becker of this laboratory, as principal investigator on prior ONR Contract No. N00014-80-C-0566, was among those contributing to our early understanding of these exciting new materials. After Dr. Becker's untimely death in 1984, J.D. Livingston became principal investigator on the present contract, with supporting work continuing at Vanderbilt University under the direction of Professor W. Flanagan.

The rapidly expanding literature on Fe-R-B compounds and magnets was reviewed, producing a systematic overview of the basic magnetic properties of $Fe_{14}R_2B$ compounds and of the relationships between processing, microstructure, and properties of Fe-R-B magnets.

The ternary ferromagnetic compound $Fe_{14}Nd_2B$ was produced by a reduction-diffusion (R-D) process involving the heating of a mixture of Fe, Nd_2O_3, and B_2O_3 powders and Ca granules. Conditions for the successful production of the desired compound were achieved with the aid of chemical, metallographic, and microprobe analysis of the resulting products. This R-D process, analogous to that used in the production of Co_5Sm magnets, was shown to have the potential of reducing raw material costs of Fe-Nd-B magnet production by about 50%.

At Vanderbilt, a Mössbauer spectrometer was purchased, and techniques for handling Fe-R-B powder samples were developed. Mössbauer spectra were measured and analyzed for a number of Fe-Nd-B and Fe-Pr-B samples prepared (at GE) by melt-spinning at various wheel speeds. Samples of Fe-Nd-B and Fe-Pr-B were prepared by plasma-arc deposition.

Section 2

REVIEW OF IRON RARE-EARTH PERMANENT MAGNETS

INTRODUCTION

The announcement in 1983 of high-performance permanent magnets based on Fe-Nd-B generated even more scientific and technological interest than the announcement 15 years earlier of Co-Sm magnets. An extensive workshop[1] on these new materials was held in Brussels in October 1984, and the Conference on Magnetism and Magnetic Materials held the following month in San Diego had over 20 papers dealing with Fe-R-B compounds. Activity continued to grow, and over 100 papers on Fe-R-B compounds were published before the end of 1985.

A review of such a fast-moving field is certain to be at least partly out-of-date before it appears in print. However, a substantial amount of information has already been generated about these new materials, and a summary of progress to date may be helpful to guide future work. We will review first what has been learned about the basic properties of the compounds on which these new magnets are based, then briefly we will describe the production and properties of magnets, and will close with a discussion of coercivity mechanisms and microstructure. This review was prepared in early 1985.

STRUCTURE

The structure of the $Fe_{14}R_2B$ phase now known to be the origin of the excellent magnetic properties has been firmly established by neutron and x-ray diffraction.[2–8] This tetragonal phase has a complex unit cell containing four formula units (68 atoms), six nonequivalent Fe sites and two nonequivalent R sites. Mirror planes normal to the c-axis contain triangular nets of Fe, Nd, and B atoms, and are separated by puckered hexagonal nets containing only Fe atoms. Similarities to the σ-phase and to Co_5R and $Co_{17}R_2$ phases have been noted. In addition to the rare-earth series from La to Lu, the phase has been found to form with Y and Th.[9] (The La compound is more difficult to form than most of the others,[10] which has led some workers to deny its existence.) Lattice parameters reported by various investigators are shown in Figure 2-1, and demonstrate the usual "lanthanide contraction." The anomalously small cell of $Fe_{14}Ce_2B$ is believed to be associated with the tetravalent, rather than trivalent, state of Ce. Figure 2-1 also shows the x-ray densities calculated from averaged values of c and a. A large anomalous thermal expansion below T_c has been observed for $Fe_{14}Y_2B$.[15,16]

CURIE TEMPERATURE

Curie temperatures reported by various investigators are shown in Figure 2-2. The differences, which are substantial in some cases, are attributed to different experimental definitions of T_c (usually unreported) and, possibly, different degrees of purity or order in the samples. Microstructure is not likely to be of importance, since T_c is normally structure-insensitive. Curie temperature is seen to peak at Gd, as with Co-R, Fe-R, and Ni-R compounds.[19]

MAGNETIZATION

The room-temperature magnetization values per unit volume reported for $Fe_{14}R_2B$ are shown in Figure 2-3. Data reported as emu/g or Bohr magnetons/formula unit were convert-

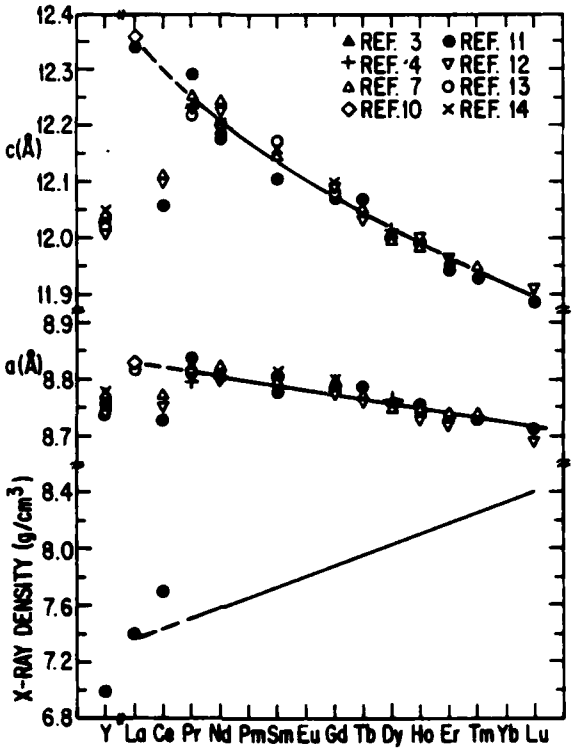

Figure 2-1. Measured lattice parameters and estimated x-ray densities of $Fe_{14}R_2B$ compounds.

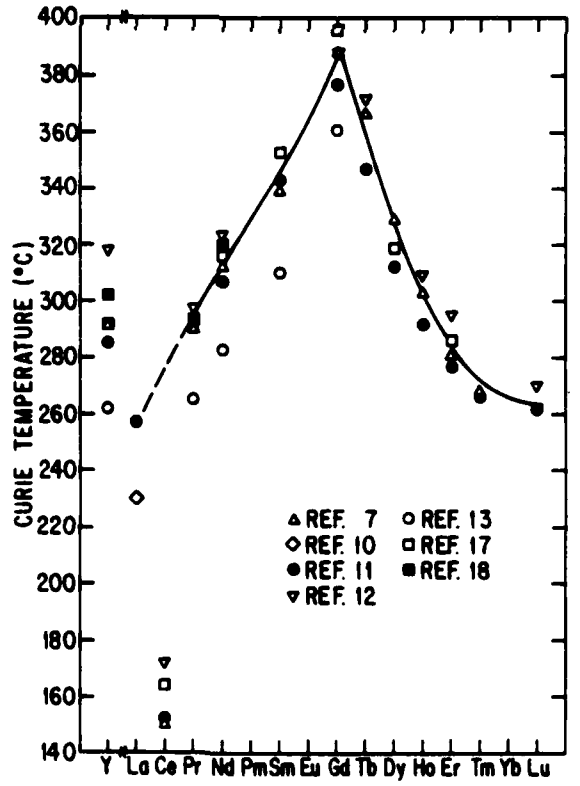

Figure 2-2. Reported Curie temperatures of $Fe_{14}R_2B$ compounds.

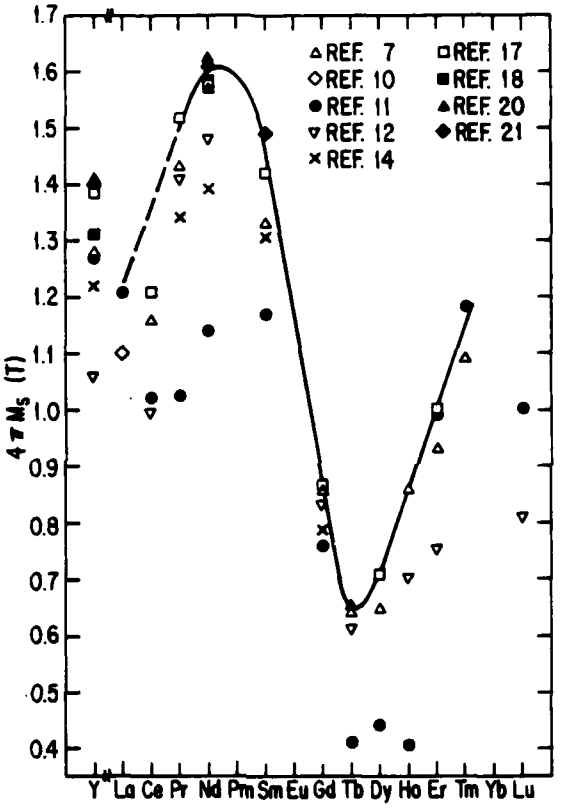

Figure 2-3. Reported magnetizations of $Fe_{14}R_2B$ compounds.

ed using x-ray densities taken from Figure 2-1. Differences here are significant and are partly caused by the different field strengths used. However, variations in the percentage of other phases and the degree of alignment in the samples were probably more important. The curve drawn in the figure gives greater weight to single-crystal data, low-oxygen samples, and the higher values.

The peak magnetization occurs for the Nd compound, in which, as for the other light rare-earths, the R net moments are coupled ferromagnetically to the Fe moments. Magnetizations are much lower for the heavy rare-earths, in which the R and Fe moments are ferrimagnetically coupled.

Neutron diffraction studies[3,4,22] have been used to determine the local moments on each of the six Fe sites and two R sites in the Nd, Pr, Y, and Dy compounds. Results have been compared[16] with theoretical calculations[23] and moments inferred from hyperfine fields at each site determined from Mössbauer measurements. A number of other Mössbauer studies have appeared.[25–32] Deciphering the complex spectra resulting from six different Fe sites is not unambiguous, but they all show a considerable variation in hyperfine field (and inferred moment) from site to site. Average Fe paramagnetic moments in several compounds have been determined by susceptibility measurements above T_c.[33]

ANISOTROPY FIELD

As in the Co-R compounds, the basic origin of the high coercivities necessary for good permanent-magnet properties is the high magnetocrystalline anisotropy. The tetragonal c-axis is the easy axis for $Fe_{14}Nd_2B$ and most other compounds in the series. Room-temperature anisotropy fields reported by various investigators are assembled in Figure 2-4. The huge

discrepancies are primarily associated with different experimental definitions of anisotropy field. Most base it on the magnetization curve taken with the field perpendicular to the easy axis of a single crystal or aligned powder sample. The anisotropy field H_A is then defined as the field where the hard-axis magnetization approaches the easy-axis magnetization value (assuming no magnetization anisotropy). In some cases this requires considerable extrapolation beyond the fields used, a process that is especially questionable when the curve is nonlinear. Considering only K_1 and K_2 terms in the anisotropy, the anisotropy field defined by proper measurement is $H_A = (2K_1 + 4K_2)/M_s$. However, any imperfection in alignment delays saturation to fields beyond H_A. Other workers[35–38] have used the "singular point detection" method, in which pulsed field is applied in the hard direction, and H_A is detected as a singularity in the curve of d^2M/dt^2 vs H.

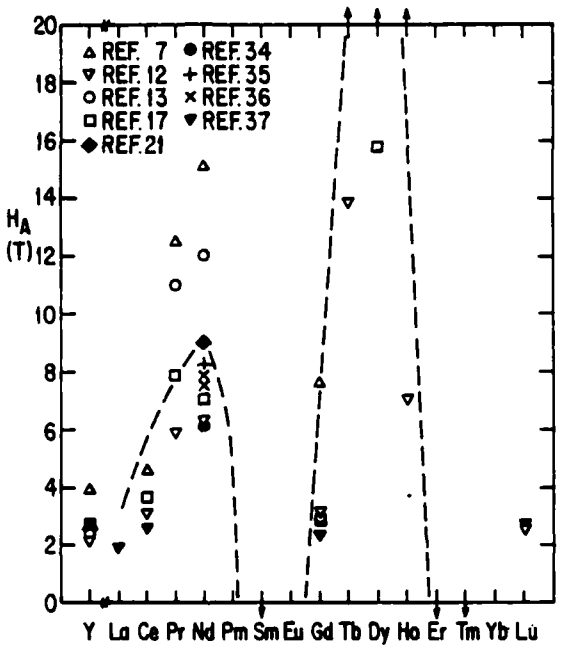

Figure 2-4. Reported anisotropy fields of $Fe_{14}R_2B$ compounds. Arrows along top indicate values above 20 T reported for R = Tb, Dy, and Ho in Reference 7. Arrows along bottom indicate negative (easy-plane) anisotropies reported for R = Sm, Er, and Tm by several investigators.

The best-established value of H_A is for $Fe_{14}Y_2B$, for which several investigators[18,20,21] have published full easy-axis and hard-axis magnetization curves for single-crystal specimens. The hard-axis magnetization curves are nearly linear ($K_2 \approx 0$), and there is no magnetization anisotropy. The room temperature H_A is 2.5 T (2 MA/m), and H_A is found to decrease with decreasing temperature. At room temperature, K_1 is about 1.1×10^7 erg/cm^3 (1.1 MJ/m^3). Since Y has no magnetic moment, this anisotropy represents the contribution of the Fe sublattice. More limited evidence suggests that H_A for $Fe_{14}R_2B$ is about 2.5 to 3.0 T for R = La, Ce, Th, and Lu, which also have no moment, and for R = Gd, which is spherically symmetric. The decrease of H_A with decreasing temperature has also been observed for La and Ce compounds,[37,38] and has been ascribed to competition between different Fe sites.

Single-crystal results for R = Nd[18,20,21] are less precise than for Y, because the hard-axis magnetization curve is nonlinear and because one author[18] reports magnetization anisotropy. However, the published curves suggest that H_A is about 9 T, with $2K_1/M_s$ about 7 T. Sagawa et al.[21] report $K_1 = 4.5 \times 10^7$ erg/cm^3 and $K_2 = 0.66 \times 10^7$ erg/cm^3. With decreasing temperature, H_A increases until about T = 150 K, where magnetization data indicate that the

magnetic symmetry is no longer easy-axis, but becomes easy-cone, with a cone angle increasing to 30° as T → 0. This "spin reorientation" has been demonstrated by various workers by magnetization or susceptibility measurements, but has not yet been confirmed by neutron diffraction.[3] Limited data indicate that H_A for R = Pr is similar, but this compound does not exhibit spin reorientation.

For the heavy rare-earths Dy and Tb, and probably for Ho, anisotropy fields are much higher. Magnetization curves for a single crystal of $Fe_{14}Tb_2B$[20] suggest that H_A may exceed 50 T. For Sm, Er, and Tm, the room-temperature anisotropy is negative, i.e., easy-plane. However, the Er and Tm compounds become easy-axis slightly above room temperature.[39] This transition has been explained in terms of the competition between the easy-axis anisotropy of the Fe sublattice and the easy-plane anisotropy of the R sublattice. The sign of the R contribution to the anisotropy has been correlated with second-order crystal field terms at the R sites.[11,15,16,40]

ALLOYING

Most practical interest has focussed on $Fe_{14}Nd_2B$ because of its high magnetization. Numerous workers have shown that replacing some of the Fe with Co leads to an enhanced Curie temperature.[7,12,41–43] Magnetization first increases slightly but then decreases after about 10% replacement. Magnetic anisotropy decreases monotonically with increasing Co, with $K_1 = 2.5 \times 10^7$ erg/cm3.5[3] for $Co_{14}Nd_2B$. (For $Co_{14}Y_2B$, anisotropy appears to be easy-plane.[41]) Replacement of the Fe with Mn or Cr leads to a decrease in T_c.[43] Additions of Al may enhance coercivity.[44]

Partial replacement of Nd by other rare-earths has also been studied. Alloying with Dy or Tb raises H_A, as expected from Figure 2-4. This leads to enhanced coercivity but decreased magnetization.[7] Replacements of Nd with mischmetal[13,37,44] or didymium[45] (a Nd-Pr-Ce mixture) have been studied as a means of producing lower-cost magnets. Effects of Y, La, and Ce replacements on $H_A(T)$[37–38] and of Y, Tb, and Ho replacements on the spin-reorientation temperature[12] have been reported. The $Fe_{14}(Y,Gd)_2B$ system has been studied to analyze induced iron moments.[46] Less attention has been paid to partial replacement of B with C and other metalloids. Absorption of hydrogen by $Fe_{14}Nd_2B$ enhances T_c and M_s, but decreases H_A.[12,19,47]

SINTERED MAGNETS

Workers from Sumitomo announced in 1983 the production of high energy product magnets from Fe-Nd-B by a process analogous to that used for Co-R magnets.[48] Castings prepared by induction melting were crushed and milled to fine powder. The powder was aligned in a magnetic field, pressed, sintered at about 1100 °C, and rapidly cooled. Coercivity was then increased by a post-sintering heat treatment at about 600 °C. They reported a maximum energy product of 36 MGOe (290 kJ/m^3), the highest achieved with any material up to that date. This magnet had a remanence of 12.3 kG (1.23 T) and an intrinsic coercivity of 12 kOe. The composition used was $Fe_{77}Nd_{15}B_8$, substantially richer in Nd and B than the stoichiometric compound. Numerous other laboratories in the U.S., Europe, China, and Japan have since successfully produced sintered Fe-Nd-B magnets. By increasing remanence, energy products up to 45 MGOe have been reported.[49,50]

Koon et al.[20] reported a saturation magnetization of 16.2 kG for a single crystal of $Fe_{14}Nd_2B$, yielding an ultimate limit of 65.6 MGOe energy product theoretically achievable with this material. The presence of other phases, porosity, and imperfect alignment in real magnets will limit energy products even if coercivity limitations are eliminated. However, energy products in the 50 to 55 MGOe range may be attainable with better metallurgical control and understanding of factors affecting coercivity.

Although record energy products are exciting, they are not needed for most applications. Of more importance in most cases are cost, resistance to demagnetization, and temperature stability of properties. As mentioned earlier, one approach to reduced cost has been to replace part or all of the Nd with didymium or mischmetal. Another is the production of polymer-bonded magnets. A reduction-diffusion (R-D) process analogous to that used for Co-R powders could also reduce costs, since rare-earth oxides rather than rare-earth metals are employed.

Addition of Dy to increase coercivity decreases irreversible losses associated with temperature rises. Li et al.[51] have documented the temperature stability of Fe-Nd-B magnets with and without such coercivity enhancement in some detail. Additions of Co also increase temperature stability, in this case via enhanced T_c.[41]

RAPID-SOLIDIFICATION PROCESSING

Although several workers had achieved substantial coercivities through the melt-spinning of Fe-R and Fe-R-B alloys prior to 1983, this approach to permanent-magnet production has been most extensively explored by the group at General Motors. They announced in 1983 the production of isotropic Fe-Nd-B magnets with a maximum energy product of 14 MGOe, remanence of 8.2 kG, and intrinsic coercivity of 15 kOe.[52,53] The composition was about $Fe_{83}Nd_{13}B_4$, slightly richer in Nd, but poorer in B, than the stoichiometric compound.

Peak properties occur at an optimum wheel speed, i.e., optimum quenching rate, that produces grains of the $Fe_{14}Nd_2B$ phase 200 to 800 Å in diameter. Good properties could also be achieved from ribbons quenched faster, i.e., at higher wheel speeds, by subsequent heat treatments that produced grain growth. Ribbons were powdered and compacted to produce dense magnets.

For other Fe-R-B alloys, only Pr gave comparable properties. Replacing part of the Nd in Fe-Nd-B with other rare-earths substantially enhanced coercivity (but decreased remanence) for Dy and Tb, but decreased coercivity for La, Ce, and Sm. The desired high-anisotropy phase was not formed when B was replaced by C, P, Si, Ge, or Al.[53,54]

The isotropic nature of the melt-spun ribbons has limited remanences and energy products. However, anisotropic magnets have recently been produced from this material by high-temperature plastic deformation. Through slip and/or twinning, a deformation texture is induced, with the c-axis tending to align along the direction of compression. In this way, remanences up to 13.5 kG and maximum energy products up to 40 MGOe have been obtained.[55]

As with sintered magnets, a variety of magnets based on rapid solidification will probably be produced, with a range of properties and prices. As past experience with Co-R, alnico, and ferrite magnets indicates, no single magnet type is likely to prove optimum for all applications.

COERCIVITY MECHANISMS

As with Co-R and ferrite magnets, it is clear that the basic origin of high coercivities in the Fe-R-B magnets is the high easy-axis magnetocrystalline anisotropy. Since coercivities remain well below the anisotropy fields, magnetization reversal apparently occurs by the nucleation and growth of reverse domains. Both reverse-domain nucleation and domain-wall pinning are governed by defects; thus coercivity is a very structure-sensitive property.

A fundamental parameter important to both nucleation and pinning aspects of coercivity is the domain-wall surface energy γ. From measurements of average surface domain width on large grains, γ for $Fe_{14}Nd_2B$ was determined[56] to be 35 erg/cm^2 (3.5×10^{-2} J/m^3). This is

similar to Co_5Y, but less than half the value for Co_5Sm. An important related parameter is the "single-domain particle diameter" $D_c = 1.4\ \gamma/M_s^2$, which is calculated to be 0.3 μm for $Fe_{14}Nd_2B$.

The parameter D_c is simply the diameter of an isolated sphere below which a single-domain structure is of lower energy at zero applied field than a two-domain structure. However, minimum energy is seldom achieved in hysteretic materials such as permanent magnets. Thus, if reverse-domain nucleation is difficult, particles with diameters considerably larger than D_c may be single-domain except when actually reversing, and particles with diameters considerably smaller than D_c will also be multi-domain while reversing. Furthermore, the calculation of D_c is relevant to an isolated sphere, not to a grain in contact with others. Nevertheless, D_c represents the size range at which wall-energy effects become important.

Sintered Fe-Nd-B magnets typically have grain diameters D = 5-15 μm. Rapidly solidified magnets have D = 200 to 800 A. Thus $D >> D_c$ for the former, and $D << D_c$ for the latter. We will therefore discuss coercivity mechanisms separately for the two types of magnets.

Sintered Magnets

Sintered Fe-Nd-B magnets share several features with Co_5Sm magnets. First, thermally demagnetized magnets, which have approached minimum energy and have several domains per grain ($D >> D_c$), have a high permeability.[48,57,58] This indicates that domain walls move easily within the grains (which is also confirmed by direct domain observations).[56,59] Second, coercivity increases markedly with increasing magnetizing field. This indicates the removal of more and more residual reverse domains that served as nuclei for reversal and limited coercivity. Finally, coercivity increases with decreasing grain size. These various observations indicate that coercivity in sintered Fe-Nd-B magnets is "nucleation-controlled" (as in Co_5Sm magnets) rather than "pinning-controlled" (as in precipitation-hardened, Cu-containing Co-R magnets).[60] This conclusion is consistent with the observation by transmission electron microscopy (TEM) that the $Fe_{14}Nd_2B$ grains are nearly defect-free.[7,58,61]

The term "nucleation" as used in these models includes the breakaway of residual reverse domains (which remain pinned at some defect), as well as the heterogeneous nucleation of reverse domains at various low-anisotropy defects such as second phases. Even in "nucleation-controlled" magnets pinning of domain walls by grain boundaries is necessary to provide a barrier to the propagation of magnetization reversal from grain to grain. Otherwise, a single weak spot in one grain would lead to reversal of the entire magnet. Thus, even "nucleation-controlled" magnets, require local pinning.[60] The pinning of domain walls by grain boundaries could involve other phases along the boundaries, or simply compositional or structural changes that lead to weakened anisotropy or exchange energies along the boundary.

High-resolution, lattice-imaging TEM of grain boundaries in sintered Fe-Nd-B magnets appears to indicate a thin (200 to 500 Å) band of b.c.c. phase separating adjacent grains of the $Fe_{14}Nd_2B$ phase.[62] In a low-coercivity sample quenched from 1080 °C, features extending into the grains that were interpreted as platelets of the b.c.c. phase were also seen. These were not seen along grain boundaries in a sample with higher coercivity that had received a post-sintering anneal at 600 °C. It was therefore suggested that the b.c.c. platelets decreased coercivity by serving as nuclei for reversed domains. Fidler[61] has also observed a thin grain-boundary layer, but identifies it as a Nd-rich phase with a d.h.c.p. structure.

Sintered magnets also generally include much larger areas, visible by optical microscopy, of a Nd-rich phase (fcc) and a B-rich phase that is probably Fe_4NdB_4.[7] The B-rich phase appears heavily faulted in TEM.[58,61] The eutectic reaction between the Nd-rich phase and $Fe_{14}Nd_2B$ is believed to enhance liquid-phase sintering. It is not clear whether the B-rich

phase plays any important role, although both it and the Nd-rich phase are nonmagnetic, and by separating $Fe_{14}Nd_2B$, grains can block the propagation of magnetization reversal. It has also been suggested[57,64] that a distribution of Nd-rich or B-rich particles within the grains may effectively reduce grain size. Some workers have also reported particles of α-Fe,[30,58,63] which could serve as domain-nucleation sites or wall-pinning sites. However, these particles have not been reported by all workers. They may represent regions in some magnets where local oxidation has decreased the metallic Nd content or diffusion times have been insufficient to remove Fe-rich regions.

As with nucleation models in other areas of materials science, e.g., in phase transformations, it is the surface-energy term that provides the energy barrier that resists breakaway of the nucleus, i.e., the reverse domain. Both the height of the energy barrier and the breakaway radius of the reverse domain decrease with increasing field. A detailed model of course depends on knowledge of the nature, size, and shape of the defect serving as the nucleation site. However, assuming that nucleation occurs when the breakaway radius decreases to the radius r of a spherical defect, the local internal field producing nucleation would be $\gamma/M_s r$. For r = 100 Å in $Fe_{14}Nd_2B$, this internal field would be 27.2 kOe. The applied field would of course be assisted by the local demagnetizing field, which will depend, among other things, on the state of reversal of neighboring grains. If, for example, the local demagnetizing field were $4\pi M_s$, the nucleation would occur at a reverse applied field of 27.2 - 16.2 = 11 kOe. This is of the order of the coercivities observed in sintered Fe-Nd-B magnets. Alloying with Dy raises coercivity substantially, probably because of an increase in K and γ, although changes in the nature of the nucleating defects may also be involved. Most nucleation sites are probably at grain boundaries, and chemical or physical changes at grain boundaries associated with heat treatment and alloying may control coercivity.

The decrease of coercivity with increasing temperature probably reflects thermal activation from nucleation sites, in addition to the decrease of K and γ with increasing temperature. Substantial thermal remagnetization was observed in an enhanced-coercivity magnet,[56] supporting a nucleation model of coercivity. Unusual hysteresis effects at cryogenic temperatures[65,66] presumably reflect the spin reorientation to easy-cone symmetry.

Production of Fe-Nd-B magnets by mixing Fe_2B, Fe, and Nd powders yielded coercivities up to 6.8 kOe.[67] A *bulk* sample of $Fe_{20}Pr_3B$ reached a coercivity of 2.5 kOe.[68] More microstructural information is needed to assess coercivity mechanisms in these cases.

Rapidly Solidified Magnets

Separation between nucleation and pinning models of coercivity is more difficult with these fine-grained magnets. For the sintered magnets, the high initial permeability after thermal demagnetization and the strong dependence of coercivity on magnetizing field were convincing evidence for nucleation-controlled coercivity. However, since $D << D_c$ for rapidly solidified (RS) magnets, most grains would not be expected to be multi-domain after thermal demagnetization, nor even be large enough to lodge residual reverse domains. Another complication is the isotropic nature of these magnets, leading to some permeability by magnetization rotation. Studies of thermally demagnetized magnets, coercivity dependence on magnetizing field, etc., for both isotropic and anisotropic RS magnets should be undertaken, but interpretation will not be as clearcut as for sintered magnets, for which $D >> D_c$.

The observation of an optimum quenching rate for peak coercivity led Croat et al.[52] to suggest that peak coercivity occurred when the grain size equalled the single-domain particle size, with underquenching and overquenching leading to reduced coercivity because of multidomain and superparamagnetic behavior, respectively.

The lowered coercivity produced by overquenching is probably not related to superparamagnetism. Using the KV = 25 kT criterion for superparamagnetism[69] indicates it will only occur at room temperature for $Fe_{14}Nd_2B$ particles with diameters less than 35 Å. Another effect, however, may limit magnetic anisotropy (and hence coercivity) as the grain size approaches the domain-wall thickness, which is about 50 Å for $Fe_{14}Nd_2B$.[70] Exchange forces across grain boundaries will oppose abrupt changes in magnetization direction, and as the grain size approaches the dimension over which this reorientation takes place, i.e., 50 Å, a significant fraction of the grain will have its magnetization rotated out of the easy axis direction. This will lead to a lower effective anisotropy and a reduced coercivity. Other possible effects of overquenching are increasing disorder of the $Fe_{14}Nd_2B$ phase and an increasing fraction of low-anisotropy amorphous phase.

The decrease of coercivity with underquenching, i.e., larger grain size, is interesting because the grain size in underquenched samples is still much smaller than in sintered magnets, which can have substantial coercivity. Possibly the grain boundaries in RS magnets are physically and/or chemically more perfect than those in sintered magnets, and are therefore less able to resist magnetization propagation from grain to grain. The Nd-rich and B-rich phases reported in sintered magnets, largely along grain boundaries, have not been reported for RS magnets, although small percentages of α-Fe and $Fe_{17}Nd_2$ have sometimes been seen.[3,25] One report[30] of decreased H_A at low wheel speeds suggests that $Fe_{14}Nd_2B$ may not fully form in underquenched samples. It will be of interest to compare the grain-size dependence of coercivity in sintered magnets and *aligned* RS magnets.

The simplest model to explain the decrease in coercivity in RS magnets with increasing grain size would consider a domain wall pinned at two grain boundaries and curved between them, its surface tension resisting expansion. The local internal field producing further reversal would again be $\gamma/M_s r$, although r would now be the radius of the grain rather than the radius of a nucleating defect. As before, r = 100 Å for $Nd_{14}Fe_2B$ yields a field of 27.2 kOe and, assuming an effective local demagnetizing field of $4\pi M_s$, a coercivity of 11 kOe. This calculation assumed an aligned magnet, with M_s and H parallel or anti-parallel. Coercivity would be somewhat higher for an isotropic magnet.

SUMMARY

The crystal structure and lattice parameters of the $Fe_{14}R_2B$ phases are well established, but more information on the ternary phase diagrams would be useful. Considerable data on T_c and M_s have been reported, but significant discrepancies exist, particularly with M_s. More consistent experimental definitions of these quantities and better specimen characterization are desirable. Discrepancies for anisotropy fields are even greater. However, careful single-crystal measurements on $Fe_{14}Nd_2B$ and $Fe_{14}Y_2B$ by several investigators have established anisotropy fields for these compounds.

Successful Fe-Nd-B magnets have been produced by two quite different techniques. Sintered magnets have grain diameters D substantially larger than D_c, the single-domain particle diameter. As in sintered Co_5Sm magnets, coercivity is controlled by reverse-domain nucleation, but grain-boundary pinning is also important. Rapidly solidified magnets have $D << D_c$, and separation between nucleation and pinning models of coercivity is more difficult. A model based on grain-boundary pinning and domain-wall curvature yields coercivities near experimental values.

ACKNOWLEDGMENTS

We are especially grateful to the many authors who provided copies of their papers prior to publication. This was especially important, since more than half of the references cited

were not yet published when this review was prepared. The author would also like to acknowledge his debt to the late J.J. Becker, who introduced the author to the field of magnetism nearly 30 years ago, and whose pioneering work in superparamagnetism, Co-R magnets, amorphous metals, and Fe-R-B magnets helped kindle the author's own interests in these subjects.

REFERENCES

1. Proc. Workshop on Nd-Fe Permanent Magnets - Their Present and Future Applications, I.V. Mitchell, ed., Commission of the European Communities, Brussels (1984).
2. J.J. Herbst, J.J. Croat, F.E. Pinkerton, and W.B. Yelon, Phys. Rev. *B29*, 4176 (1984).
3. J.F. Herbst, J.J. Croat, and W.B. Yelon, J. Appl. Phys. *56* (to be published).
4. J.F. Herbst and W.B. Yelon, J. Appl. Phys. *56* (to be published).
5. D. Givord, H.S. Li, and J.M. Moreau, Solid State Commun. *50*, 497 (1984).
6. C.B. Shoemaker and D.P. Shoemaker, Acta Cryst. *C40*, 1665 (1984).
7. M. Sagawa, S. Fujimura, H. Yamamoto, Y. Matsuura, and K. Hiraga, IEEE Trans. Magn. *MAG-20*, 1584 (1984).
8. H. Boller and H. Oesterreicher, J. Less Common Metals *103*, L5 (1984).
9. K.H.J. Buschow, Ref. 1.
10. H.H. Stadelmaier, N.C. Liu, and N.A. ElMasry, Materials Letters (to be published).
11. S. Sinnema, R.J. Radwanski, J.J.M. Franse, D.B. de Mooij, and K.H.J. Buschow, J. Magn. Magn. Mater. *44*, 333 (1985).
12. C. Abache and H. Oesterreicher, J. Appl. Phys. *56* (to be published); H. Oesterreicher, F. Spada, and C. Abache, Mater. Res. Bull. *19*, 1069 (1984).
13. Y.C. Yang, H.Y. Chen, Z.X. Liu, B. Liao, F. Xing, and W.W. Ho, J. Appl. Phys. *56* (to be published).
14. M.Q. Huang, E. Oswald, E. Boltich, S. Hirosawa, W.E. Wallace, and E. Schwak, Physica B and C (to be published).
15. D. Givord, H.S. Li, J.M. Moreau, R. Perrier de la Bathie, and E. du Tremolet de Lacheisserie, Physica B and C (to be published).
16. D. Givord and H.S. Li, Ref. 1.
17. E.B. Boltich, E. Oswald, M.Q. Huang, S. Hirosawa, W.E. Wallace and E. Burzo, J. Appl. Phys. *56* (to be published).
18. D. Givord, H.S. Li, and R. Perrier de la Bathie, Solid State Commun. *51*, 857 (1984).
19. H.R. Kirchmayr and C.A. Poldy, J. Magn. Magn. Mater. *8*, 1 (1978).
20. N.C. Koon, B.N. Das, M. Rubinstein, and J. Tyson, J. Appl. Phys. *56* (to be published).
21. M. Sagawa, S. Fujimura, H. Yamamoto, Y. Matsuura, and S. Hirosawa, J. Appl. Phys. *56* (to be published).
22. D. Givord, H.S. Li, and F. Tasset, J. Appl. Phys. *56* (to be published).
23. B. Szpunar and J.A. Szpunar, J. Appl. Phys. *56* (to be published).
24. R. Kamal and Y. Anderson, (to be published).
25. F.E. Pinkerton and W.R. Dunham, Appl. Phys. Lett. *45*, 1248 (1984).
26. F.E. Pinkerton and W.R. Dunham, J. Appl. Phys. *56* (to be published).
27. H. Onodera, Y. Yamaguchi, H. Yamamoto, M. Sagawa, Y. Matsuura, and H. Yamamoto, J. Magn. Magn. Mater. *46*, 151 (1984).
28. H.M. van Noort, D.B. de Mooij, and K.H.J. Buschow, J. Appl. Phys. *56* (to be published).
29. J.M.D. Coey, J.M. Cadogan, and D.H. Ryan, Ref. 1.
30. R. Grossinger, G. Hilscher, H. Kirchmayr, H. Sassik, R. Strnat, and G. Wiesinger, Physica B and C (to be published).

31. M. Rosenberg, P. Deppe, M. Wojcik, and H. Stadelmeier, J. Appl. Phys. (to be published).
32. J.W.C. deVries, R.C. Thiel, and K.H.J. Buschow, Phys. Rev. B (to be published).
33. E. Burzo, E. Oswald, M.Q. Huang, E. Boltich, and W.E. Wallace, J. Appl. Phys. *56* (to be published).
34. F. Spada, C. Abache, and H. Oesterreicher, J. Less-Common Metals *99*, L21 (1984).
35. G. Asti, F. Bolzoni, F. Leccabue, L. Pareti and R. Panizzieri, Ref. 1.
36. R. Grossinger, P. Obitsch, X.K. Sun, R. Eibler, H.P. Kirchmayr, F. Rothwarf, and H. Sassik, Materials Letters *2*, 539 (1984).
37. R. Grossinger, X.K. Sun, R. Eibler, and H.R. Kirchmayr, this conference.
38. X.K. Sun, R. Grossinger, R. Eibler, and H.R. Kirchmayr, Physica B and C (to be published).
39. S. Hirosawa and M. Sagawa, Solid State Commun. (to be published).
40. J.M. Cadogan and J.M.D. Coey, Phys. Rev. *B30*, 7326 (1984).
41. Y. Matsuura, S. Hirosawa, H. Yamamoto, S. Fujimura, and M. Sagawa, Appl. Phys. Letters *46*, 308 (1985).
42. R.A. Overfelt and J.J. Becker, Appl. Phys. Letters *44*, 925 (1984).
43. Y.C. Yang, W.W. Ho, H.Y. Chen, J. Wang, and J. Lan, J. Appl. Phys. *56* (to be published).
44. Z. Maocai, M. Deqing, J. Xiuling, and L. Shiqiang, this conference.
45. M. Okada, S. Sugimoto, C. Ishizaka, T. Tanaka, and M. Homma, J. Appl. Phys. *56* (to be published).
46. E. Burzo, Acta Phys. Polonica (to be published).
47. K. Oesterreicher and H. Oesterreicher, phys. stat. sol. (a) *85*, K61 (1984).
48. M. Sagawa, S. Fujimura, M. Togawa, H. Yamamoto and Y. Matsuura, J. Appl. Phys. *55*, 2083 (1984).
49. K.S.V.L. Narasimhan and B.M. Ma, IEEE Trans. Magn. (to be published).
50. K.S.V.L. Narasimhan, *J. Appl. Phys. 56 (to be published).*
51. D. Li, H.F. Mildrum, and K.J. Strnat, J. Appl. Phys. *56* (to be published).
52. J.J. Croat, J.F. Herbst, R.W. Lee, and F.E. Pinkerton, Appl. Phys. Letters *44*, 148 (1984).
53. J.J. Croat, J.F. Herbst, R.W. Lee, and F.E. Pinkerton, J. Appl. Phys. *55*, 2078 (1984).
54. Y.F. Tao and G.C. Hadjipanayis, J. Appl. Phys. *56* (to be published).
55. R.W. Lee, Appl. Phys. Letters (to be published); R.W. Lee, E.G. Brewer, and N.A. Schaffel, 1985 Intermag Conference.
56. J.D. Livingston, J. Appl. Phys. *56* (to be published).
57. A. Handstein, J. Schneider, D. Stephan, W. Fischer, U. Heinecke, R. Grossinger, H. Sassik, and H.R. Kirchmayr, Mater. Lett. (to be published).
58. G.C. Hadjipanayis, K.R. Lawless, and R.C.Dickerson, J. Appl. Phys. *56* (to be published).
59. D. Li and K.J. Strnat, J. Appl. Phys. *56* (to be published).
60. J.D. Livingston, J. Appl. Phys. *52*, 2544 (1981).
61. J. Fidler, 1985 Intermag Conference.
62. K. Hiraga, M. Hirabayashi, M. Sagawa, and Y. Matsuura, Japan. J. Appl. Phys. *24*, L30 (1985).
63. J. Fidler, P. Skalicky, M. Sagawa, and Y. Matsuura, Proc. 8th Europ. Cong. on Electron Microscopy, Budapest (1984) Vol. I, p. 811.
64. H.H. Stadelmaier, N.A. ElMasry, N.C. Liu, and S.F. Cheng, Materials Letters *2*, 411 (1984).
65. R. Grossinger, H.R. Kirchmayr, R. Krewenka, K.S.V.L. Narasimhan, and M. Sagawa, this conference.

66. K.J. Strnat, D. Li, and H. Mildrum, this conference.
67. H.H. Stadelmaier, N.A. ElMasry, and S.R. Stallard, J. Appl. Phys. *56* (to be published).
68. H.H. Stadelmaier, N.A. ElMasry, and S. Cheng, Materials Letters *2*, 169 (1983).
69. C.P. Bean and J.D. Livingston, J. Appl. Phys. *30*, 120S (1959).
70. T. Suzuki, K. Hiraga, and M. Sagawa, Japan. J. Appl. Phys. *23*, L421 (1984).

Section 3

PRODUCTION OF $Fe_{14}Nd_2B$ BY A REDUCTION-DIFFUSION PROCESS

INTRODUCTION

The announcements in 1983 of the development of Fe-Nd-B magnets by Sumitomo [1] and General Motors[2] generated widespread scientific and technological activity.[3,4] Remanences and maximum energy products of Fe-Nd-B magnets are substantially higher than those of Co_5Sm magnets, and the materials costs are lower. However, widespread application to industrial devices (particularly motors) will not be accomplished without further technical developments directed at lowering the cost of production. Using metals as starting materials, the raw materials cost is dominated by the cost of Nd metal. If, instead, Nd_2O_3 is used and reduced with Ca, raw material costs would be substantially lowered. The objective of the present work is to study the production of $Fe_{14}Nd_2B$, the desired ferromagnetic compound, by a Ca reduction-diffusion (R-D) process.

The R-D Process

The Co_5Sm powders used to produce the earliest rare-earth magnets were ground from ingots made by melting and casting cobalt and samarium metals. However, in 1969 R.E. Cech of the General Electric Research and Development Center invented the R-D process to produce Co_5Sm.[5–7] In this process cobalt powder, calcium granules, and rare-earth oxide powder are blended together and reacted under hydrogen at 1150°C. The calcium reduces the samarium oxide and the samarium metal diffuses into the cobalt. The reduction can be represented by the equation:

$$R_2O_3 + 10Co + 3Ca \xrightarrow[3\ hr]{115\ °C,\ H_2} 2RCo_5 + 3CaO$$

After cooling, the excess calcium and calcium oxide are removed from the reacted product by hydrating with wet nitrogen followed by washing with water and dilute acid.

The main advantages of the reduction-diffusion process are the use of relatively inexpensive rare-earth oxide as raw material and the direct production of alloy powder suitable for milling. However, the calcium and oxygen content of this powder is higher than in alloys made by melting. Co_5Sm magnets produced from R-D powder have properties comparable to those produced from melt-cast powder.[8] Because of its substantially lower cost, the R-D process has become the major commercial means of producing cobalt rare-earth powders for permanent magnets.[9–13]

An analogous process to produce $Fe_{14}Nd_2B$ by the Ca reduction of Nd_2O_3 and B_2O_3 could be represented by the equation:

$$2Nd_2O_3 + B_2O_3 + 28Fe + 9Ca \rightarrow 2Fe_{14}Nd_2B + 9CaO$$

Alternatively, B could be introduced in another form, such as ferroboron.[14]

Cost Analysis

Currently, at a very early stage of commercialization, Fe-Nd-B magnets with simple shapes and loose dimensional tolerances sell for about $90/lb or $3/MGOe. Similar cobalt-samarium magnets cost about $3.75/MGOe; ferrites, 25 to 50 cents; and alnico, $2.20.[15] It seems clear that at higher production volumes, and with the attendant cost reductions Fe-Nd-B will enjoy a major portion of the current $80 million world rare-earth cobalt magnet market[16] (except where high-temperature capability is required). Much greater cost reductions will be required for significant substitutions of the ferrite and alnico market and for the replacement of electromagnets, notably in the automative industry. If this occurs, an annual market greater than $800 million is projected.[17]

While the raw material costs do not currently dominate the cost of finished magnets, they do play a substantial role, and they control the ultimate lowest cost achievable. Thus, there has been substantial analysis of the availability and costs of raw materials.[18-19] The availability of raw materials far exceeds any envisioned requirements but increases in primary processing capacity will be required. The costs will depend on the processing route followed. The comparison made here will be between (1) the direct melt process starting with Fe, Nd and B metals and (2) the reduction-diffusion process starting with Nd_2O_3, Ca, Fe and Fe-B (ferroboron) or B_2O_3.

Currently, Nd metal sells for $25/lb in large quantities and is projected to remain in the $20 to $25/lb range. At similar quantities Nd_2O_3 sells for $5/lb and may go as high at $6/lb in the future. In the R-D process calcium is a significant cost at $5.50/lb. Iron and ferroboron costs are the same for both processes, $.29 and $1.35/lb, respectively.

At a $5 oxide cost and a 90% recovery, the R-D process produces a pound of magnet material for $3.60 of raw materials cost. For $6 oxide, there is a $4.00/lb raw material cost.

At $25/lb for Nd metal the melt process requires $8.65/lb of magnet. At $20/lb for Nd the cost is $7.00.

The raw materials costs differ by about a factor of two between the two processes and the melt process is significantly more sensitive to the neodymium cost. On the other hand, the R-D process materials cost is almost equally sensitive to the cost of calcium as it is to the cost of Nd_2O_3.

Table 3-1 compares the raw materials cost and three magnet selling prices. It can be seen that at current magnet prices, the raw materials costs play an insignificant role. However, if the magnet price is to reach a level low enough to stimulate large demand, then the raw materials costs and the process route become very significant.

Table 3-1

COSTS (DOLLARS PER POUND) OF Fe-Nd-B MAGNETS

Raw materials cost	R-D process, 3.80; melt process, 7.80
Current selling price	90.00
Japanese projected selling price	30.00
Required selling price for substantial replacement of ferrite and alnico	18.00

PROCESS RUNS

The various steps in the R-D process used are shown in Figure 3-1. The original target composition was chosen to be 75 at% Fe, 15 at% Nd, 10 at% B, close to that reported by Sumitomo[1] to produce optimum sintered magnets. (This is considerably richer in Nd and B than the stoichiometric $Fe_{14}Nd_2B$ compound, which is 82.3 at% Fe, 11.8 at% Nd, and 5.9 at% B.) The amount of Ca required to reduce the Nd_2O_3 and B_2O_3 was calculated, and then augmented by 30 or 50% to ensure the presence of excess Ca.

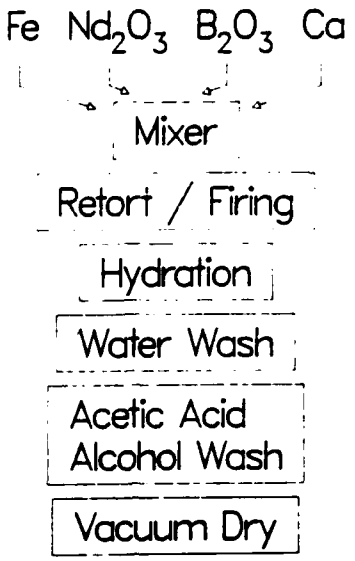

Figure 3-1. Steps in R-D process used to produce $Fe_{14}Nd_2B$.

Mixing

The starting materials used were 99.9% purity Fe, 6-9 μm size; 99.9% purity Nd_2O_3, 2 μm size; 99% purity Ca, 1-3 mm shot; fused B_2O_3, ground by mortar and pestle to obtain fine powder. The ingredients were weighed and loaded into a powder blender, where they were thoroughly mixed. The blended powder was then loaded into an iron boat with a loosely fitting cover.

Firing

The reduction process was performed in an electrically heated furnace in a hydrogen atmosphere. Firing times and temperatures were varied from 2 to 16 hours and from 1100 to 1200 °C. After firing, the iron boat was moved to a cooling chamber and purged with argon. It was removed for hydration after reaching room temperature.

Hydration

The iron boat now contained a hard sintered block of material bluish-gray in color. The block was placed in a pyrex tray and inserted into a glove box containing a moist argon atmosphere. It is believed the following two reactions take place:

$$CaH_2 + H_2O \rightarrow CaO + 2H_2$$

and $$CaO + H_2O \rightarrow Ca(OH)_2$$

Both reactions are exothermic and result in a change in the shape of the material, which eventually falls to a fine powder. The time required for hydration was usually 3 to 4 days.

Water Wash

The powder was then placed in a beaker of chilled water and mechanically agitated to dissolve the lime. The Fe-Nd-B-rich slurry was allowed to settle to the bottom of the beaker, with the lime staying suspended in solution and subsequently removed by decanting. The process was continued until the solution was fairly clear. Throughout the water-washing process, which is exothermic, the temperature was monitored and maintained between 15 and 20 °C.

Acid Wash

The residual lime was dissolved using a dilute solution of acetic acid. During the acid wash, the pH was monitored and kept between 6 and 7. The powder was stirred during the washing procedure, which was continued until the pH stabilized. The solution was decanted, and the powder was given a water rinse followed by a methanol rinse.

Vacuum Drying

The moist powder was then placed in a heated desiccator and dried overnight at a maximum temperature of 40 °C. When dry, the powder was sampled for analyses and stored in closed, air-free containers.

Results

For the seven R-D processing runs conducted, Table 3-2 shows the firing time and temperature and the initial (weighed) and final (wet chemical analyses) compositions of the powder. The input composition of Ca was augmented (beyond that calculated to be required for reduction) by 30% for runs RD-1 and RD-2 and by 50% for the remaining runs.

Table 3-2

COMPOSITION RESULTS FOR R-D PROCESS RUNS

Run	Time (hr)	Temp (°C)	Input Composition wt% (at%)			Output Composition wt%			
			Fe	Nd	B	Fe	Nd	B	Ca
RD-1	2	1100	64.8 (75)	33.5 (15)	1.67 (10)	65.81	25.9	1.19	3.54
RD-2	4	1140	64.8 (75)	33.5 (15)	1.67 (10)	68.92	28.74	1.41	0.26
RD-3	4	1140	61.18 (71.9)	36.96 (16.8)	1.86 (11.3)	65.56	30.34	1.78	0.39
RD-4	6	1140	54.2 (68)	44.18 (21.5)	1.62 (10.5)	65.0	33.6	1.64	0.23
RD-5	8	1200	54.2 (68)	44.18 (21.5)	1.62 (10.5)	59.78	34.5	1.3	1.43
RD-6	4	1140	64.7 (74)	33.4 (14.8)	1.9 (11.2)	69.1	29.06	1.9	0.18
RD-7	16	1140	64.7 (74)	33.4 (14.8)	1.9 (11.2)	60.8	28.7	1.44	4.25

The first run, RD-1, was performed for 2 hours at 1100 °C. Analysis for oxygen content yielded 0.63 to 0.78%, which was satisfactorily low. However, the wet chemical analysis indicated a loss of Nd and B.

Time and temperature for run RD-2 were increased to 4 hours and 1140 °C to achieve a more complete reaction. Oxygen content of the product powder was about 0.1%. Yields of Nd and B were increased, but output concentrations were still significantly lower than input concentrations.

To compensate for the loss of Nd and B, input concentrations of Nd and B were increased for run RD-3. The Ca excess was also increased from 30 to 50%. The output composition still was Nd-poor compared to the target composition.

For run RD-4, the input concentration of Nd was increased still further, and reaction time increased from 4 to 6 hours. The output composition was now very close to the original target composition.

Run RD-5 was performed with the same input composition as RD-4, but at 1200 °C, to see if increased temperature would improve Nd yield. Although the Nd yield was improved, the resulting material was a hard brick that resisted hydration.

For run RD-6, the time and temperature and approximate input composition of RD-2 were used. Several 1 mm-dia. Fe wires were inserted into the mixed powder, to allow later microstructural study of the diffusion reaction of B and Nd with Fe. To understand the source of Nd loss, compositions were analyzed at an intermediate step in the wash process. After the water wash, the powder composition, by weight percent, was 65.37 Fe, 30.15 Nd, 1.77 B, 1.93 Ca. After the acid wash and drying, it was 69.11 Fe, 29.06 Nd, 1.90 B, and 0.18 Ca. The acid wash apparently preferentially removed Nd, decreasing the Nd/Fe ratio from 0.46 to 0.42. Analysis of the filtered sediment in the decanted fluid from the water wash yielded 2.34 wt% Fe, 13.96 wt% Nd. The water wash apparently also preferentially removes Nd.

Microstructural study of the powder and the iron wires from run RD-6, reported below, suggested that 4 hours at 1140 °C had not allowed sufficient diffusion and reaction time to produce a homogeneous product. Run RD-7 was therefore performed with the same temperature and input composition, with firing time increased from 4 to 16 hours. The resulting product was not only more homogeneous, but had a higher Nd/Fe ratio. The output and input Nd/Fe ratios, by weight percents, are plotted in Figure 3-2. The data show clearly that for fixed input composition, Nd output is improved by increasing firing time and/or temperature. For similar firing conditions, fractional loss of Nd appears to be higher for higher Nd/Fe input ratios.

Runs 1, 5, and 7 were high in Ca because the product was hard and did not hydrate and wash well. The oxygen associated with the Ca can account for most of the shortfall in total weight percent.

METALLOGRAPHY

Although chemical analyses reveal the overall composition of the product powders, they are insufficient to determine whether the desired $Fe_{14}Nd_2B$ phase was being produced. Powders from each run were therefore also analyzed by optical microscopy and x-ray diffraction. Iron wires inserted in the powder for runs RD-6 and RD-7 were examined by optical microscopy and electron microprobe to determine the extent of the diffusion reaction of B and Nd with Fe.

R-D Powders

The $Fe_{14}Nd_2B$ phase can be easily distinguished from the other phases present in the Fe-Nd-B system by polarized-light microscopy, because of its characteristic magnetic domain patterns that are revealed through the Kerr effect.[20] In most of the R-D runs, some powder par-

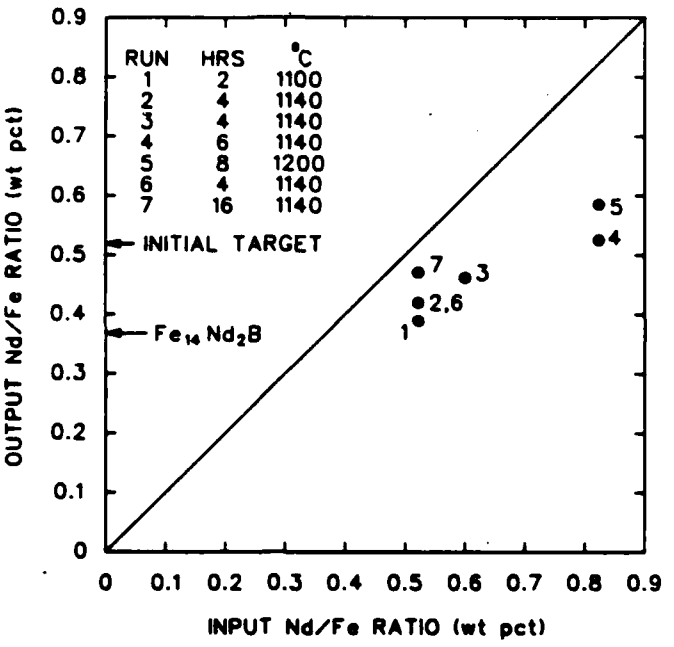

Figure 3-2. Input and output Nd/Fe ratio, by weight percent, for seven R-D processing runs at times and temperatures shown. Run RD-7 showed the least Nd loss.

ticles were found that consisted primarily of $Fe_{14}Nd_2B$ (e.g., Figures 3-3 and 3-4). Such particles are often much larger than the original Fe powder, indicating that the process involves not just diffusion of B and Nd into Fe, but diffusive transfer of Fe as well. In addition to particles such as those in Figures 3-3 and 3-4, many particles have complex microstructures in which $Fe_{14}Nd_2B$, when present, was only one of several phases (e.g., Figures 3-5 to 3-7). Those results indicated considerable inhomogeneity of composition, with many particles having compositions far different from the average powder composition.

These observations, plus similar observations on Fe wires (reported below), suggested that longer times at the reaction temperature were required to allow interdiffusion to produce greater homogeneity. This was confirmed by observations on the powder produced by run RD-7, which was reacted for 16 hours at 1140 °C (compared to 4 hours for run RD-6). In this powder, the $Fe_{14}Nd_2B$ phase occupied over 90% of the observed area, far more than the powders from the earlier runs. Much of the product consisted of single-crystal particles of $Fe_{14}Nd_2B$ (Figure 3-8), but a substantial fraction had partially sintered into polycrystalline agglomerates (Figure 3-9). Higher magnification micrographs of these latter regions (Figure 3-10) show a Nd-rich phase in the vicinity of the $Fe_{14}Nd_2B$ grain boundaries. This phase melts well below the reaction temperature, and its presence in the final microstructure suggests that a Nd-rich liquid between the $Fe_{14}Nd_2B$ particles promoted the partial sintering. As noted earlier, the target composition for the R-D runs was chosen to match that used by Sumitomo for their sintered magnets. Their composition contains more Nd than the stoichiometric $Fe_{14}Nd_2B$ so that Nd-rich liquid can accelerate sintering, and a Nd-rich phase is present in their sintered magnets.[1,3]

Polycrystalline agglomerates such as seen in Figure 3-9 would be undesirable in magnet production, in which the magnetic alignment of single-crystal particles is a crucial step. However, milling of the R-D product would probably break up these partly sintered agglomerates into mostly single-crystal particles.

Figure 3-3. Large $Fe_{14}Nd_2B$ particle produced in run RD-4. Polarized light. Magnetic domain structure indicates easy magnetic axis (tetragonal c-axis) is normal to surface.

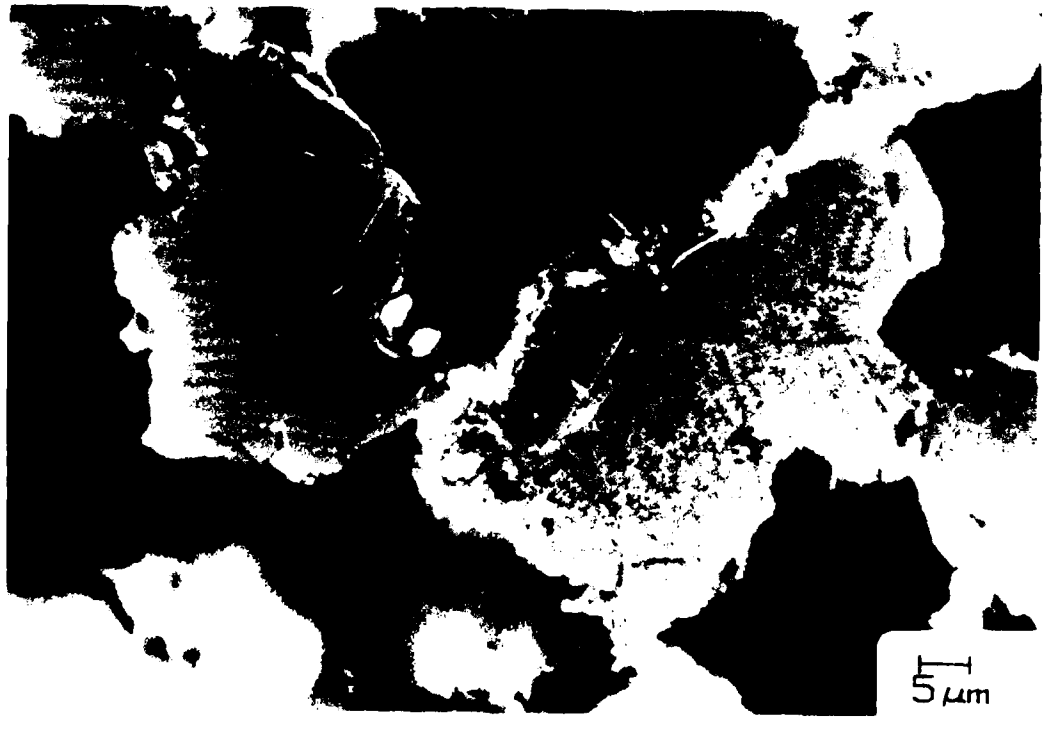

Figure 3-4. $Fe_{14}Nd_2B$ particles produced in run RD-2. Polarized light. Magnetic easy axis normal to surface in particle on right, nearly horizontal in particle on left.

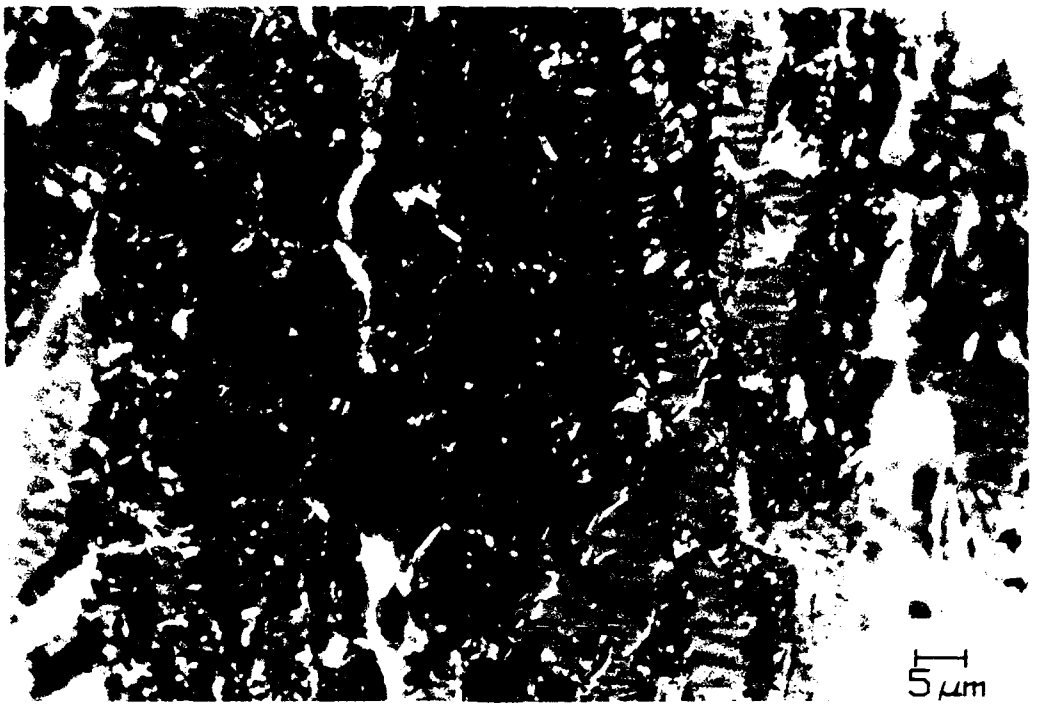

Figure 3-5. Large multiphase particle produced in run RD-4. Polarized light.

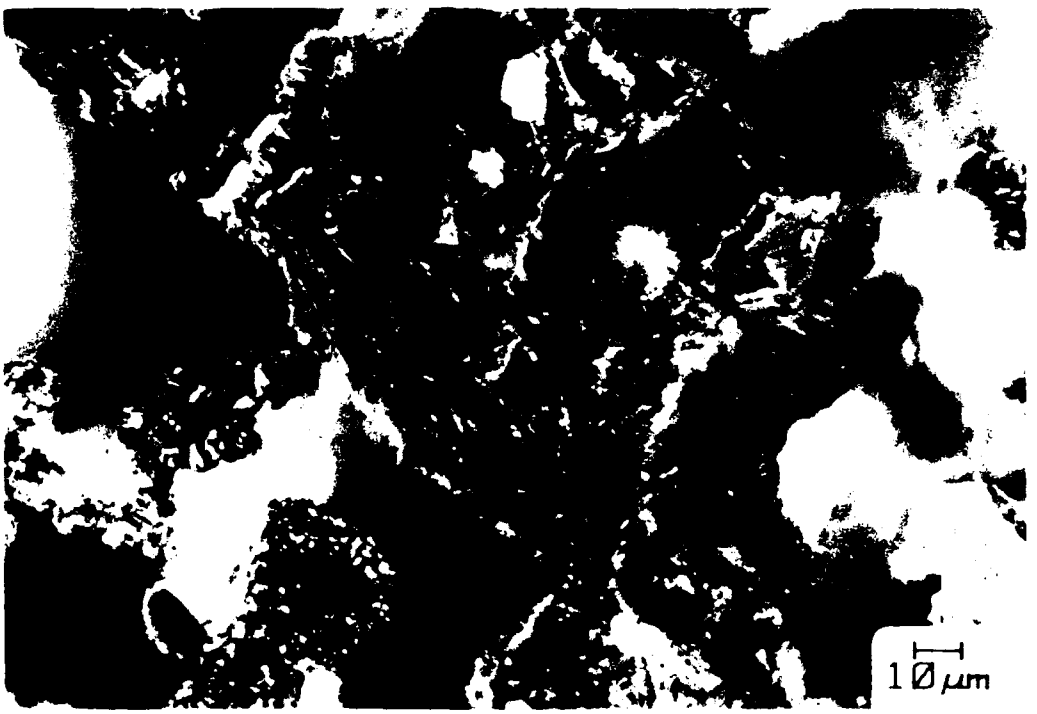

Figure 3-6. Multiphase particle produced in run RD-6. Polarized light.

Figure 3-7. Multiphase particle produced in run RD-6. Bright field.

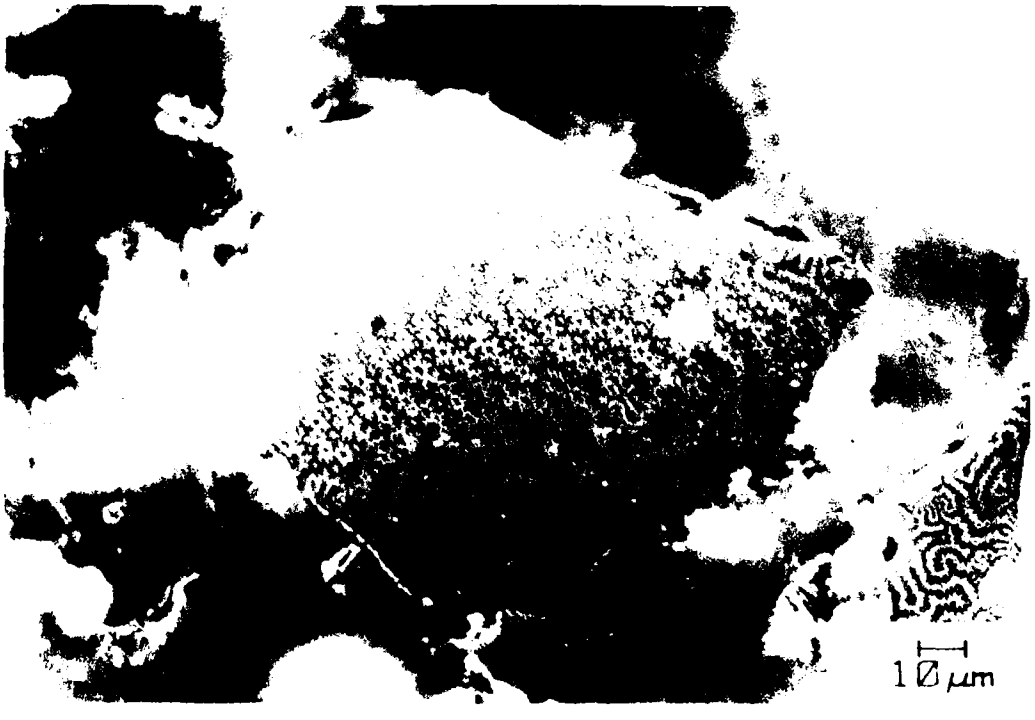

Figure 3-8. $Fe_{14}Nd_2B$ particle typical of most of powder produced in run RD-7. Polarized light.

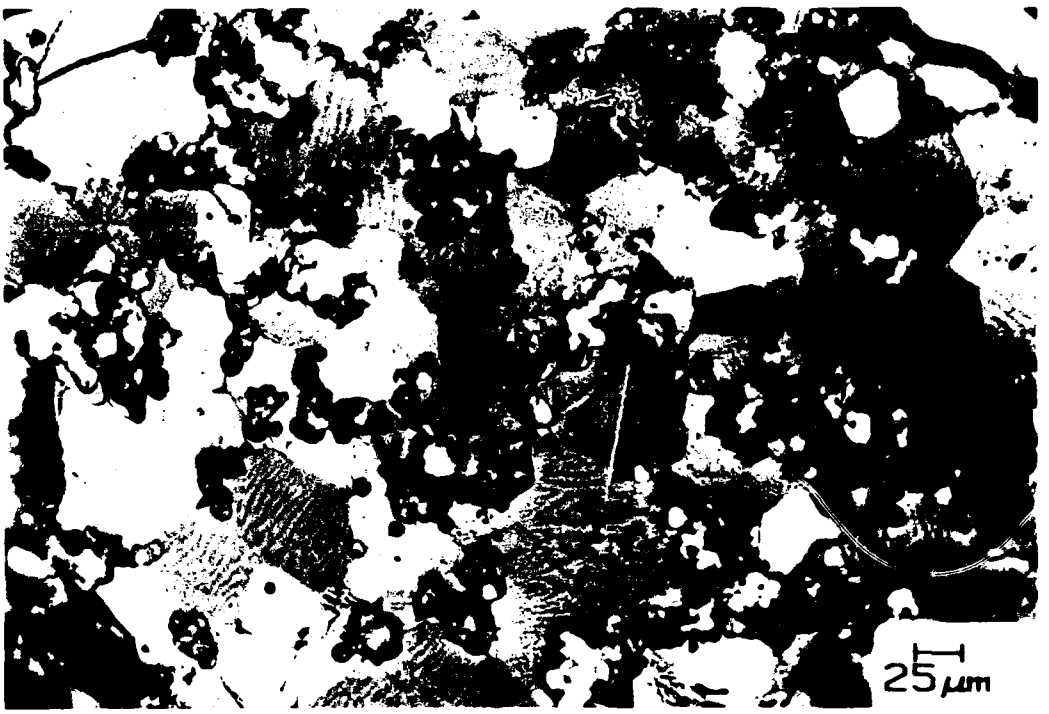

Figure 3-9. Partly-sintered agglomerate of $Fe_{14}Nd_2B$ grains produced in run RD-7. Polarized light.

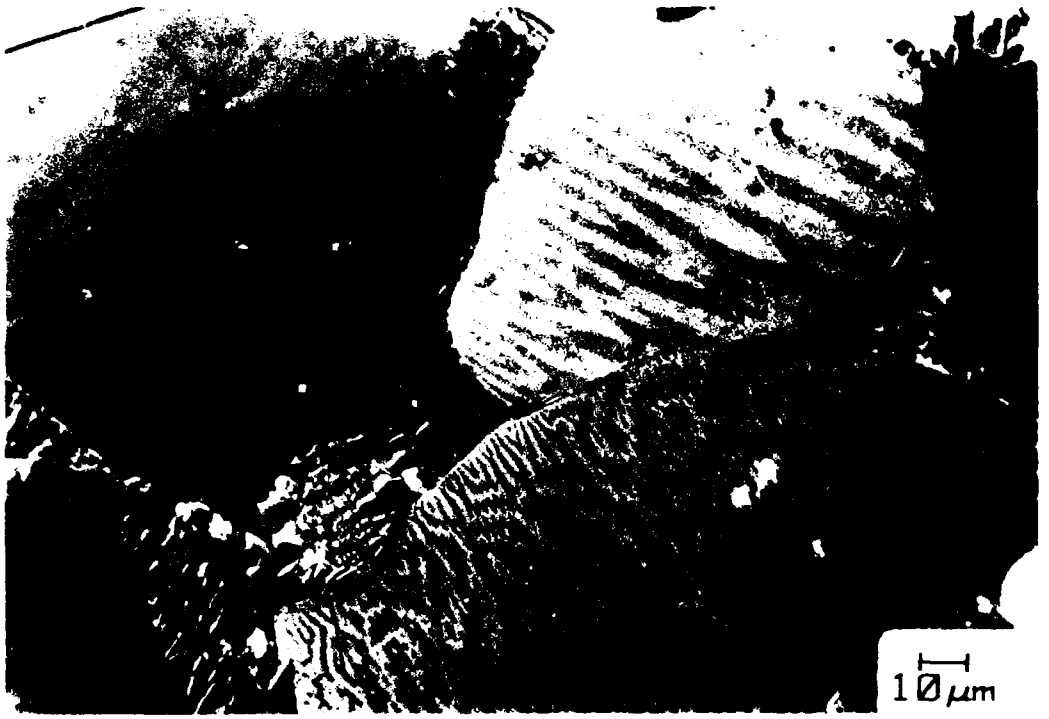

Figure 3-10. Higher-magnification of agglomerate showing Nd-rich phase along and near $Fe_{14}Nd_2B$ grain boundaries. Polarized light.

X-ray diffraction patterns were taken of powders from each of the runs, generally yielding very complex patterns with a multitude of lines. In most cases, some of the lines could be indexed to strong lines of the tetragonal $Fe_{14}Nd_2B$ structure, but many could not be. Some were indexable as Fe, Fe_2B, or $Ca(OH)_2$ lines, and some were not identified. The pattern that most closely matched a published pattern for the $Fe_{14}Nd_2B$ phase[21] was that of RD-7 powder that had been given an extra water wash. Prior to this extra wash, $Ca(OH)_2$ lines were strong enough to obscure many of the $Fe_{14}Nd_2B$ lines. In summary, the x-ray results indicate that only the RD-7 powder consisted primarily of the desired $Fe_{14}Nd_2B$ phase, which is consistent with the metallographic observations described above.

Wires

In runs RD-6 and RD-7, 1 mm-diameter iron wires were inserted in the powder mixture before reaction to get a better understanding of the reaction diffusion of B and Nd into Fe. Metallographic examination of the wire from run RD-6 revealed that most of the wire interior was unreacted iron. An irregular reaction zone varying from a few microns up to as much as 100 μm thick was seen along the wire peripheries. In some areas, deep penetration of $Fe_{14}Nd_2B$ grains was observed (Figure 3-11), but the $Fe_{14}Nd_2B$ grains were generally accompanied by another phase, believed to be Fe_2B. In a few areas, a eutectic microstructure (probably Fe-Fe_2B) was seen (Figure 3-12). In contrast, the wires from run RD-7, reacted at the same temperature but for a longer time, showed a surface reaction zone consisting almost exclusively of $Fe_{14}Nd_2B$. A micrograph and corresponding Nd x-ray map show that the Nd concentration drops abruptly at the Fe-$Fe_{14}Nd_2B$ boundary except for some penetration along Fe grain boundaries (Figure 3-13). Microprobe analysis indicates an average Nd concentration of about 28 wt% in the compound, whereas ideal stoichiometry would be about 27 wt%. A line trace across the reaction layer indicates a variation of at most 0.4 wt% Nd from the outside (Nd-rich) to the border with the Fe (Nd-poor).

Figure 3-11. Edge (at bottom) of 1 mm-dia. iron wire inserted in run RD-6. Includes Fe_2B phase as well as $Fe_{14}Nd_2B$. Polarized light.

Figure 3-12. Eutectic region in iron wire inserted in run RD-6. $Fe_{14}Nd_2B$ grain at bottom center. Polarized light.

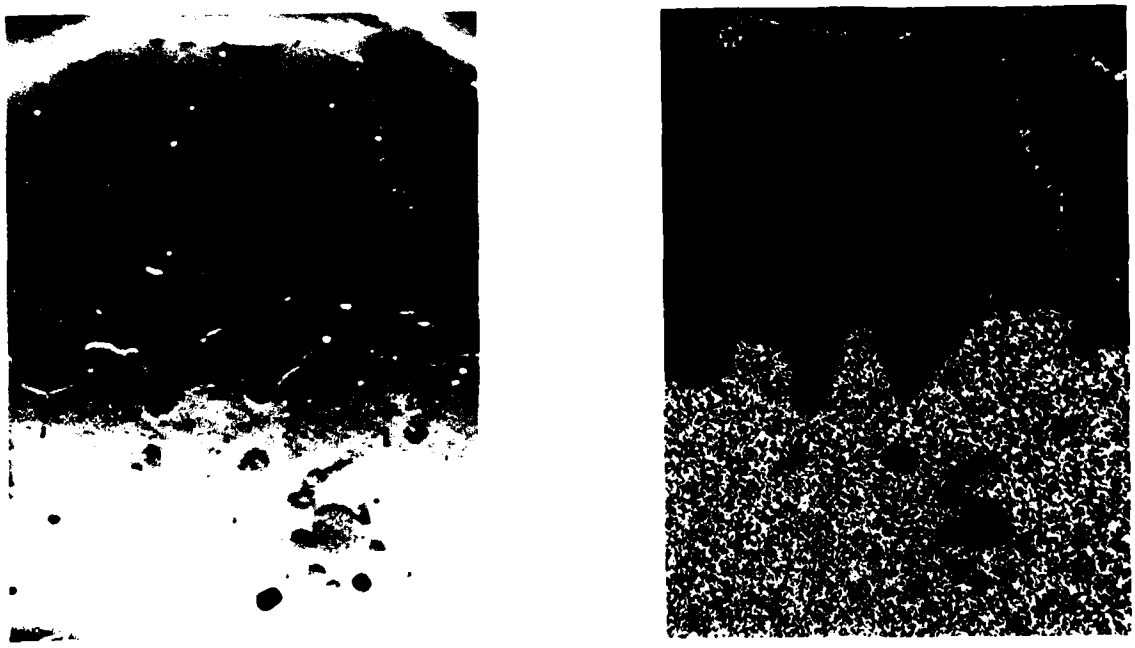

(a) (b)

Figure 3-13. Edge (at bottom) of iron wire inserted in run RD-7. (a) SEM, (b) Nd x-ray map shows Nd in boundary $Fe_{14}Nd_2B$ phase and along Fe grain boundaries.

In the interior of the RD-7 wire, many regions showed a grain-boundary phase (Figure 3-14) that is Nd-rich (Figure 3-15). This was occasionally seen in the RD-6 wire, but it was much rarer and penetration was more limited. In much of the RD-7 wire, the Nd-rich boundary phase was observed all the way to the center of the wire. These various observations of the wires from runs RD-6 and RD-7 suggest that the reaction and diffusion of B into Fe usually precedes the diffusion of Nd, and that both B and Nd preferentially diffuse along Fe grain boundaries.

CONCLUSIONS

Production of a ternary compound like $Fe_{14}Nd_2B$ by the R-D process is inherently more complex than production of a binary compound like Co_5Sm. Inhomogeneities in the initial powder mixture, and different reaction and diffusion rates for the B and Nd, make it difficult to produce a homogeneous ternary product of the desired composition. Metallographic observations showed that after most of the experimental runs, the resulting powders were very inhomogeneous in microstructure and, by inference, in composition. This suggested using a longer time at temperature to allow further diffusion to produce homogenization, and run RD-7, held 16 hours at 1140 °C, produced a product consisting primarily of $Fe_{14}Nd_2B$. The feasibility of using the R-D process to produce this compound was, therefore, successfully demonstrated. During the course of this study, other groups have successfully used an R-D process to produce $Fe_{14}Nd_2B$.[14,22]

A major problem noted from the chemical analyses was a loss of Nd, particularly in the washing steps. According to Herget,[14] this results from a corrosive reaction between water and the Nd-rich phase, and can be avoided by replacing water with a proprietary organic solvent. The Nd loss can presumably also be reduced by minimizing the amount of Nd-rich phase in the final product. This is consistent with the data in Figure 3-2, which show lower Nd loss for a more homogeneous product (run RD-7) and higher loss at higher Nd/Fe input ratios (runs RD-4 and RD-5). This suggests that it may be preferable to make R-D powder near to the stoichiometric composition of the compound, thereby minimizing the amount of Nd-rich phase. This would also decrease the problem of premature sintering (Figures 3-9 and 3-10). A Nd-rich sintering aid could then be added to the R-D powder before aligning and sintering into magnets.

In summary, the production of $Fe_{14}Nd_2B$ by the R-D process is inherently more complex than the production of Co_5Sm, but this process has been successfully demonstrated. Reduction in raw materials costs with the process are less dramatic than for Co_5Sm, but can become important when and if magnet prices are reduced substantially below current levels. Metallographic studies indicate the importance of having sufficient time at the firing temperature to allow diffusion to produce a homogeneous product. The problem of Nd loss in the washing steps is apparently associated with the Nd-rich phase and could be reduced by producing $Fe_{14}Nd_2B$ powder with near-stoichiometric composition.

ACKNOWLEDGMENTS

R-D processing was done by Bob Zabala; Lyman Johnson and Charles McFarland made significant contributions. Metallography was done by Curt Rodd and Estelle Sauter, microprobe analysis by Karleen Davis, and x-ray diffraction by Don Marsh and Paul Shields. Wet chemical analysis was done by Winifred Balz and oxygen analysis by Ted Evenden.

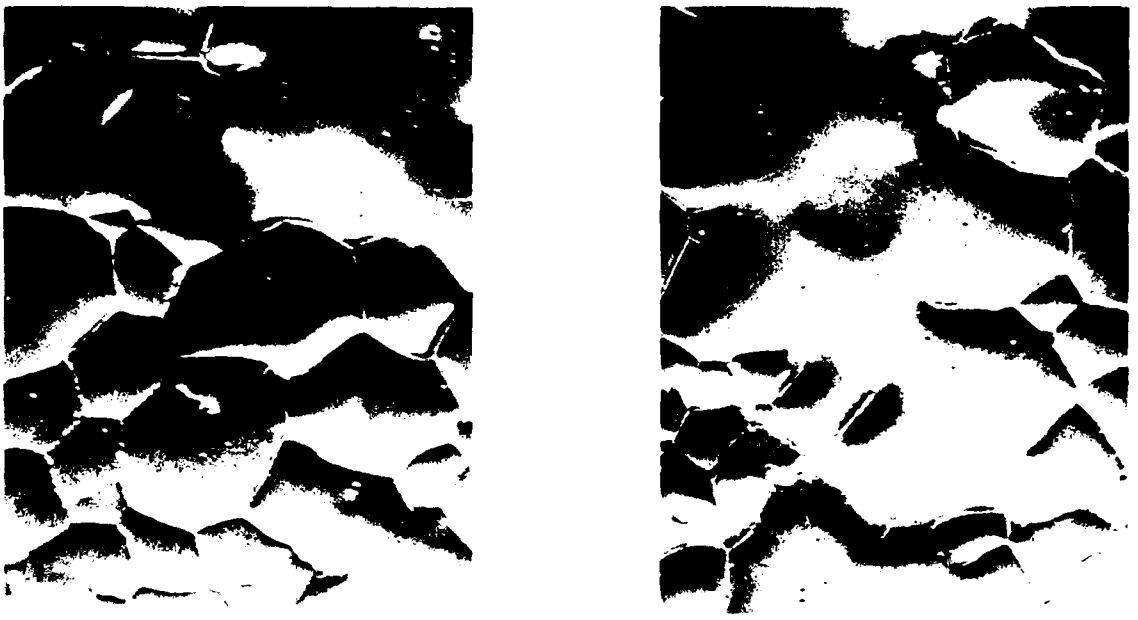

(a) (b)

Figure 3-14. Interior of iron wires from run RD-7, showing phase along Fe grain boundaries. SEM.

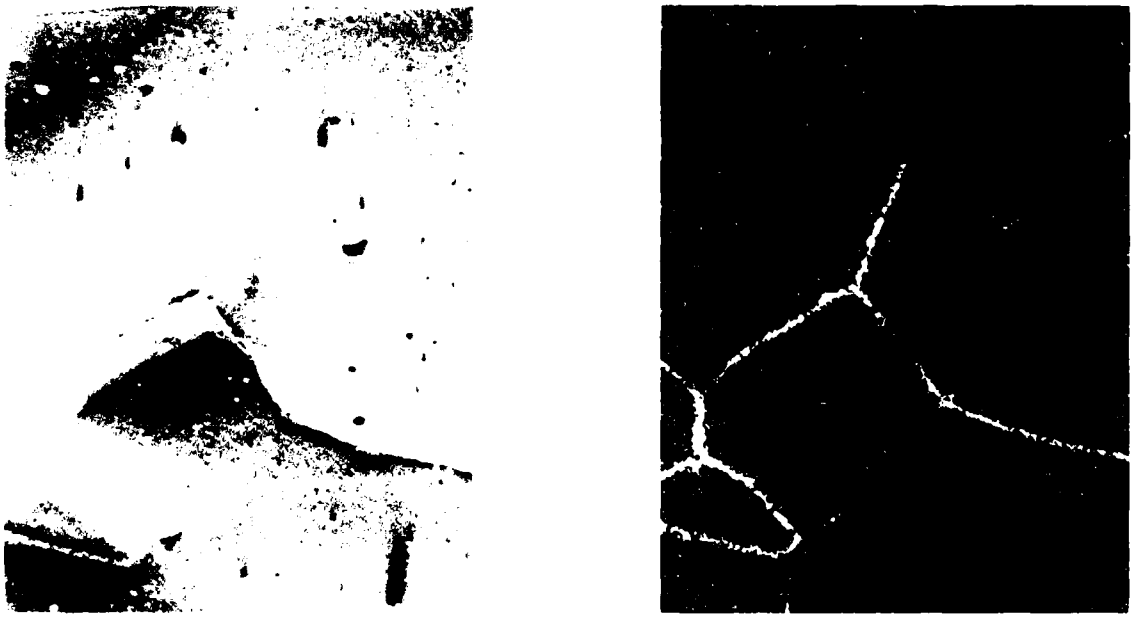

(a) (b)

Figure 3-15. Interior of iron wire from run RD-7. (a) SEM (b) Nd x-ray map, showing phase along Fe grain boundaries is Nd-rich.

REFERENCES

[1] M. Sagawa, S. Fujimura, M. Togawa, H. Yamamoto, and Y. Matsuura, J. Appl. Phys. *55*, 2083 (1984).

[2] J. J. Croat, J. F. Herbst, R. W. Lee, and F. E. Pinkerton, *ibid*, p. 2078.

[3] J. D. Livingston, Proc. 8th Internat. Conf. on Rare-Earth Magnets and their Applications, Karl J. Strnat, ed., Univ. of Dayton, Dayton, Ohio (1985) p. 423.

[4] A. L. Robinson, Science *223*, 920 (1984).

[5] R. E. Cech, "Rare Earth Intermetallic Compounds by a Calcium Hydride Reduction-Diffusion Process." U.S. Patent 3,748,193, July 24, 1973.

[6] R.E. Cech, "Rare Earth Intermetallic Compounds Containing Calcium," U.S. Patent 3,826,696, July 30, 1974.

[7] R.E. Cech, "Cobalt-Rare Earth Intermetallic Compounds Produced by Calcium Hydride Reduction of Oxides," J. Metals *26*, No. 2, 32 (1974).

[8] D.L. Martin, R.P Laforce, A.C. Rockwood, C.M. McFarland, and L. Valentine, "The Properties of Permanent Magnets Made From Reduction-Diffusion Cobalt-Rare Earth Powders," Proc. 10th Rare Earth Research Conf., 105 (1973).

[9] C.M. McFarland, "Cobalt-Rare Earth Powders by the Reduction-Diffusion Process," Proc. 10th Rare Earth Research Conf., 692 (1973).

[10] F.G. Jones, J.H. Thoe, H.E. Lehman, and R.B. Downs, "Production of RCo_5 and R_2Co_7 Powders by the R/D Process," Proc. 12th Rare Earth Research Conf., 1054 (1976).

[11] C. Herget and H.G. Domazer, "Methods for the Production of Rare Earth-3d Metal Alloys with Particular Emphasis on the Cobalt Alloys," Goldschmidt informiert 4/75, No. 35, P. 3.

[12] Y. Chengzhou, Y. Qiming, D. Xiuxuan, G. Qinghai, and D. Baozhen, "Research and Production of SmCo Powder by Calciothermic Process," Proc. 7th Internat, Workshop on Rare Earth-Cobalt Permanent Magnets and Their Applications, China Academic Publishers (1983) p. 439.

[13] T.S. Krishnan and C.K. Gupta, "Production and Fabrication of Rare Earth-Cobalt Permanent Magnets," ibid, p. 467.

[14] C.Herget, Dayton Conference (see Ref. 3) p. 407.

[15] J.W. Fiepke, Machine Design, 1/10/85, p. 93.

[16] P.G. Boswell, Proceedings of European Communities Workshop on Nd-Fe Permanent Magnets, Brussels, October 1984, I.V. Mitchell, ed, p. 57.

[17] ibid p. XVI.

[18] ibid p. 13-66.

[19] Dayton Conference (see Ref. 3).

[20] J.D. Livingston, J. Appl. Phys. *57*, 4137 (1985).

[21] H. Boller and H. Oesterreicher, J. Less - Common Metals *103*, L5 (1984)

[22] G. Sun, Y. Xiao, S. Zhou, and L. Yuan, Paper 5Pd 1 at International Conference on Magnetism, San Francisco, August 1985.

Section 4

WORK AT VANDERBILT

INTRODUCTION

The work reported in this section has been done by Collin Anderson, working with Professor William F. Flanagan of the Department of Mechanical and Materials Engineering. It is a continuation of the PhD research performed by Dr. R.A. Overfelt, at GE-CRD* and at Vanderbilt University, on rapidly solidified iron-based rare-earth alloys, which have high intrinsic magnetic coercivities (Hc_i).[1] In that study, a variety of alloys were prepared using the melt-spinning apparatus at GE-CRD, and their magnetic properties were measured using a vibrating-sample magnetometer (VSM). Systematic variation of wheel speeds and compositions (i.e., quenching rates) showed that Hc_i was maximum for a wheel speed, V_s, of 20 m/s, and for an alloy composition $Fe_{76}R_{16}B_8$, where R represents the rare-earth elements Pr or Nd. Other light rare-earths were not as effective, though some provided higher remanence. It was found that C and Si proved to be no substitute for B, and Co raised the curie temperature when partially substituted for Fe. TEM observations showed that the resulting grain size for the "optimal" wheel speed was $\approx$50 nm, much less than the critical size for stabilizing a single magnetic domain.

It has been established that the phase responsible for such high coercivity has a Curie temperature $T_c \cong 300$ °C, is tetragonal (having a single easy axis of magnetization with a high crystalline anisotropy), and has the composition $Fe_{14}R_2B$.[1-5] The initial magnetic permeabilities that were observed suggest that the coercivity is controlled by reverse-domain nucleation and growth. The large crystalline anisotropy and the small grain size support this view. The presence of crystal interfaces (grain boundaries) and defects confound sophisticated theoretical analysis of experimental observations, but are expected to play an important role in the coercivity mechanism.

While the magnetically "hard" phase is $Fe_{14}R_2B$, the optimum alloy for high coercivity is $Fe_{76}R_{16}B_8$, an alloy having a higher percentage of rare-earth and boron. This manifests itself in the presence of a rare-earth rich grain boundary phase in the underquenched materials.

It is not surprising that an "optimal" quench-speed exists. As the wheel speed goes above the optimal value of 20 to 30 m/s, the grain size decreases, approaching the domain-boundary width size, and in addition, increasing amounts of the amorphous magnetically soft phase forms, both of which lead to lower values for Hc_i. For cooling rates below the optimal value where the resulting grain size increases, the reason for the drop in coercivity is less obvious. One explanation has been offered by J.D. Livingston as arising from grain boundary pinning,[6] and this is strongly influenced by the chemical and structural detail of the boundaries.

EXPERIMENTAL APPROACH

The work at Vanderbilt is intended to study the nature of the boundaries and the boundary phases in the rapidly solidified magnetic alloys. The initial work, which is covered by this contract, focuses on the use of Mössbauer and VSM techniques to study these alloys. The Mössbauer spectrometer and ^{57}Co source, and the computer facilities used for data acquisition

* This study evolved from the work of J.J. Becker at GE-CRD and was carried out in collaboration with him.

and processing were purchased under this contract. A vibrating-sample magnetometer was built at Vanderbilt; it has a maximum magnetizing field of ±12 kOe, which is inconvenient for studying samples with saturation fields beyond this range. When this happens, the samples are initially saturated by cooling from above the Curie temperature in a 5 kOe magnetizing field. A difficulty arises when Hc_i exceeds the 12 kOe limit, in which case, simple extrapolation through the second quadrant is used to determine Hc_i. (It is hoped that a larger magnet will be obtained for future work.)

The Mössbauer and VSM measurements were made on samples rapidly solidified by melt-spinning and by plasma-spray processing. Also, normally cast ingots were studied. Future work would involve samples prepared by direct reduction techniques and by deep-undercooling using the 100 M drop tube at NASA's Marshall Space Flight Center in Huntsville, Alabama. These treatments provide various (metastable) microstructures, and coupled with annealing treatments, allow one to study a range of processing variables.

EXPERIMENTAL RESULTS

Figure 4-1 gives Mössbauer spectra for an $Fe_{76}Pr_{16}B_8$ ingot and for $Fe_{76}Pr_{16}B_8$ melt-spun ribbons that were solidified at various wheel-surface speeds (V_s). Representative hysteresis loops are provided in Figure 4-2a-d. As can be seen, the highest coercive force was obtained when V_s = 20 m/s.* Figure 4-3 shows a similar series of spectra for the Nd alloy. The coercive forces corresponding to these wheel speeds are given in Table 4-1. Figures 4-4 and 4-5 show the effect of annealing an overquenched sample containing either Pr (Figure 4-4) or Nd (Figure 4-5).

Least squares fitting was performed on Mössbauer spectra for wheel-surface speeds ranging from 0 m/s (ingot) to 80 ms. The fitting parameters of the tetragonal phase do not vary substantially with V_s. Table 4-2 lists the results of such fits for two representative samples. A computer least-squares fit (Gradient Method) of the Mössbauer spectrum of such a sample (Figure 4-1c) indicates the presence of the hard tetragonal phase and perhaps a small amount of paramagnetic phase (Figure 4-6). These curve-fitting results will be discussed in greater detail below.

Table 4-3 lists the coercivities of some plasma-arc deposited samples. Coercivities were measured on as-deposited samples and on a deposited material that was annealed at various temperatures. Representative hysteresis loops are given in Figure 4-7. The fact that the magnetic hardness of the as-deposited sample increased upon annealing indicates that the samples were overquenched. Since the cooling rate of plasma-arc samples decreased with increasing deposition thicknesses, thicker deposits will likely have increased coercivities. This method of magnet production is currently being explored.

DISCUSSION

It was hoped that Mössbauer spectroscopy could be used to conclusively identify all phases present in the Fe-R-B (R = Pr,Nd,Sm) permanent magnets. Unfortunately, Mössbauer spectra resulting from these alloys are extremely complex. The magnetically hard $Fe_{14}R_2B$ tetragonal phase alone contributes 36 lines, thereby making it very difficult to isolate lines contributed by other phases. However, Mössbauer spectra interpretation can still provide quite useful phase information.

There are 68 atoms in the tetragonal $Fe_{14}Re_2B$ unit cell. Fifty-six of the 68 atoms are Fe, and there are six different nonequivalent Fe sites in the unit cell. Each site is in a different magnetic and electrical environment, and therefore the electronic energy levels of the Fe

* The wheel speed of 20 m/s is referred to as "optimal," while specimens quenched at lower or higher speeds are referred to as "underquenched" and "overquenched," respectively.

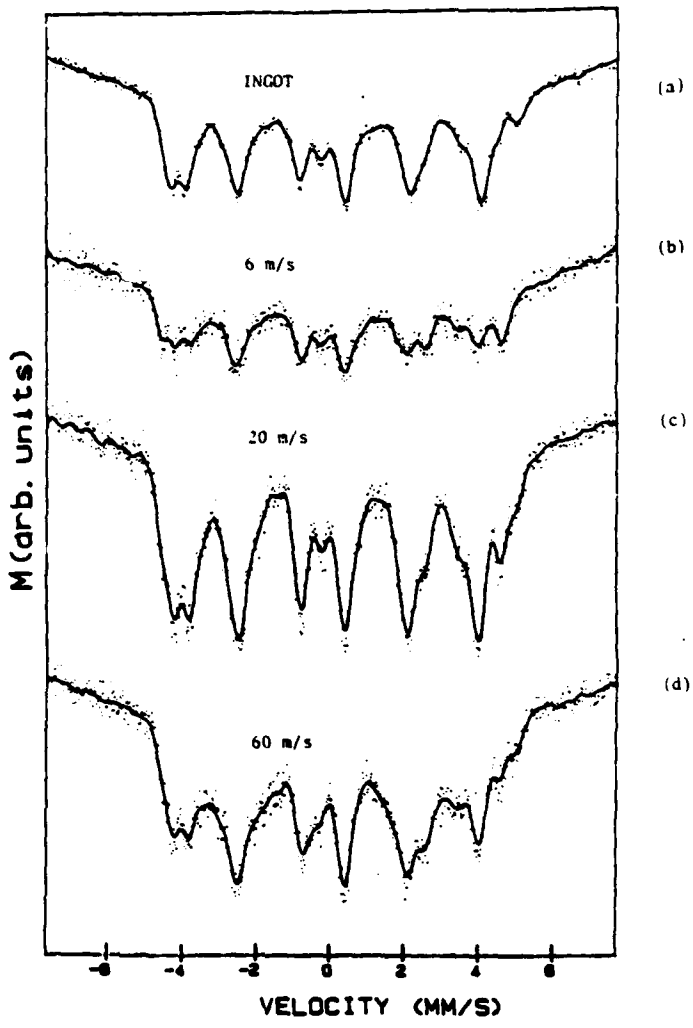

Figure 4-1. Mössbauer spectra for $Fe_{76}Pr_{16}B_8$; (a) ingot; (b) (c), and (d) melt-spun ribbons produced with various wheelspeeds. V_s = 20m/s yields the largest Hci.

atoms are different for each site. Because Fe is ferromagnetic, each site contains a magnetic hyperfine field, which splits the energy levels of the ground and the first excited states of each site in such a way as to allow six possible transition energies between these two states for each site. Thus, each site contributes six lines to an $Fe_{14}Re_2B$ Mössbauer spectrum. The 56 Fe atoms occupy the six sites in the ratio of 16:16:8:8:4:4 for the so-called k1, k2, j1, j2, c and e sites, respectively; so, the relative intensities of these sites in a Mössbauer spectrum should be in the same ratio. For a randomly oriented sample, the intensity of the six lines associated with each site should be in the ratio 3:2:1:1:2:3.

A computerized least-squares fit of a sample of $Fe_{76}Pr_{16}B_8$ quenched at a wheel speed of 20 m/s is shown in Figure 4-3. The spectrum is analyzed as containing lines from the tetragonal phase (36 lines) and possibly a paramagnetic phase (1 or 2 lines), so a 38-line fit was attempted. The position parameters found by the program for the tetragonal phase agree reasonably with those found in the literature (see Table 4-2). However, the site and line intensities found by the program do not reflect the theory described above. Possible preferred orientation in the samples would explain the lack of a 3:2:1:1:2:3 ratio among the individual

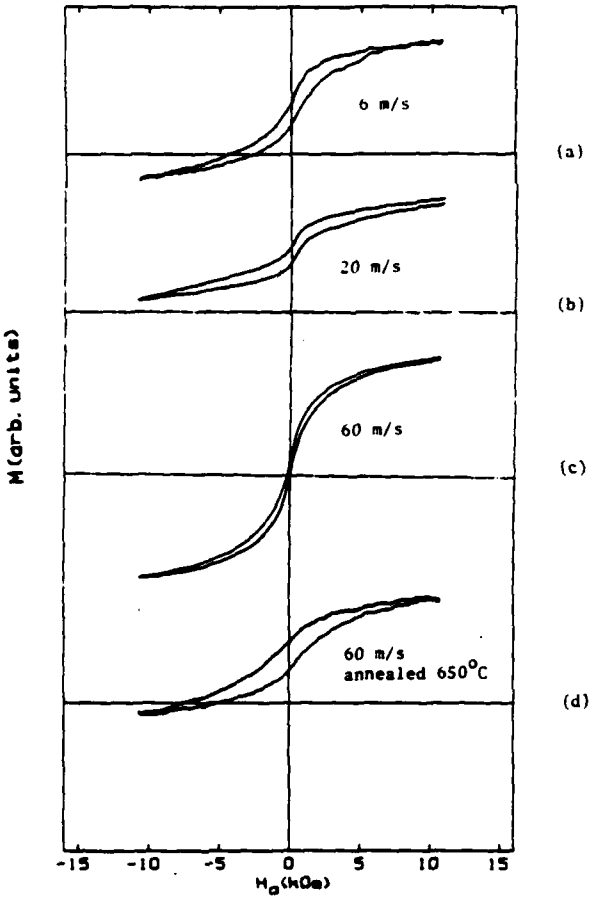

Figure 4-2. Hysteresis loops for $Fe_{76}Pr_{16}B_8$ for V_s equal to (a) 6m/s (b) 20m/s and (c) 60 m/s. (d) shows the curve obtained when (c) is annealed at 650 °C for 25 minutes.

lines within a site.[9] The absence of 16:16:8:8:4:4 ratio among the sites is less easily explained, but it is not particularly surprising in light of the spectrum complexity. Many workers constrain the site and line intensities to the ratios given above. Such constraints tie the fit more closely to the physical picture but appear to less accurately reflect the data.

The integrated intensity of all the absorption peaks should be related to the ^{57}Fe content of the samples. It is apparent that this is not true from Figures 4-1 and 4-3 to 4-5, since all the samples were made to have approximately the same Fe content. This can be explained by the effect of lattice defects or strains on the Mössbauer recoiless fraction, f.[10] Annealing overquenched samples causes the integrated intensity to more than double. As one might expect, this indicates that such defects or lattice strains may be important. This, as well as the effect of crystallographic texture of the samples, will be studied in future work, when Mössbauer experiments at various temperatures and under various magnetic fields will be attempted.

Figure 4-8 shows Mössbauer spectra found in the literature[11] for (a) Nd_2Fe_{17} by itself, (b) a mixed-phase spectra of Nd_2Fe_{17} and $Fe_{14}Nd_2B$, and (c) $Fe_{14}Nd_2B$ by itself. These spectra illustrate, qualitatively, the changes that occur in experimental spectra and they help in interpreting them. It is important to note that substituting another rare-earth element such as Pr for Nd has almost no effect on shape of the Mössbauer spectrum of the tetragonal phase.

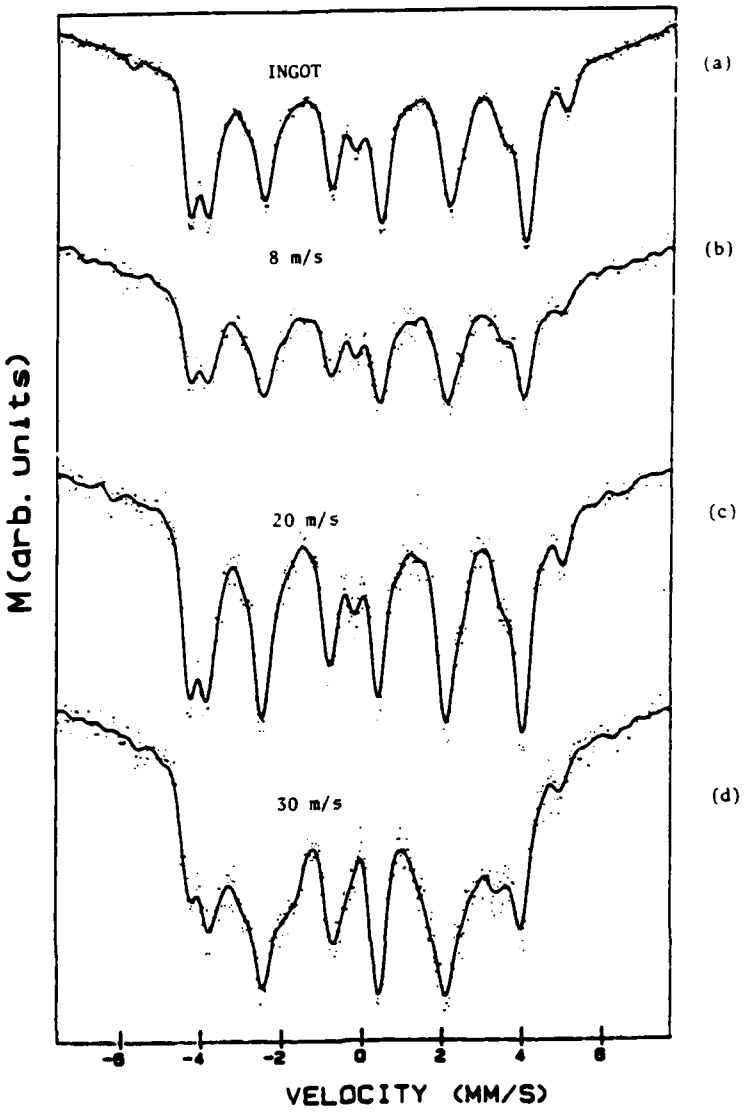

Figure 4-3. **Mössbauer spectra for $Fe_{76}Nd_{16}B_8$ (a) ingot (b) (c), and (d), melt-spun ribbons produced with various wheel speeds. V_s = 20m/s yields the largest Hci.**

Table 4-1

Hc_iO FOR VARIOUS V_s

	Wheel Speed	Hc_i
$Fe_{76}Pr_{16}B_8$	6 (N/S)	4.3 kOe
	20	14.40*
	60	0.22
	80	0.16
	60 (annealed at 650 °C 20 min)	7.48
	80 (annealed at 650 °C 20 min)	1.34
$Fe_{76}Nd_{16}B_8$	8	9.09
	20	18.7*
	30	14.2*

*Extrapolated

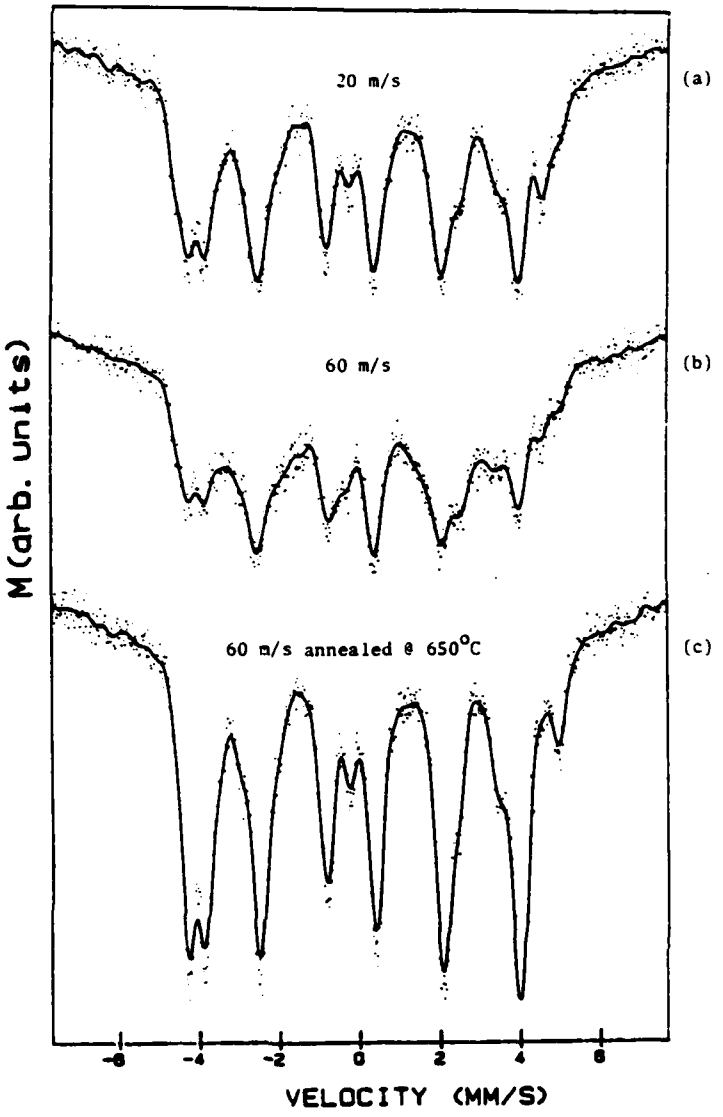

Figure 4-4. Mössbauer spectra for a melt-spun $Fe_{76}Pr_{16}B_8$ (a) optimally quenched (20m/s) (b) overquenched (60m/s) and (c) overquenched and annealed at 650 °C for 25 minutes.

Changing the rare-earth element primarily affects only the overall width of the spectrum by changing the internal fields at the Fe sites.[8]

As can be seen, the optimally quenched $Fe_{76}Pr_{16}B_8$ spectrum (Figure 4-1c) looks very much like the tetragonal-phase spectrum (Figure 4-8c). The only discrepancy in the two spectra is the small peak appearing at a Doppler velocity around −0.3 mm/s in Figure 4-1c. This strong resemblance provides further evidence that the ribbons quenched at a wheel speed, V_s, equal to 20 m/s contain only the hard tetragonal phase and possibly a tiny amount of some paramagnetic phase, which would account for the additional peak.

The spectrum for an overquenched (V_s = 50 m/s) material given in Figure 4-1d is very similar to the mixed-phase spectrum of Nd_2Fe_{17}, which contributes 36 lines (Figure 4-8b). Based on this similarity, it is assumed that the overquenched ribbons contain $Fe_{14}Nd_2B$ and one other ferromagnetic phase at room temperature; one can conclude that the phases present

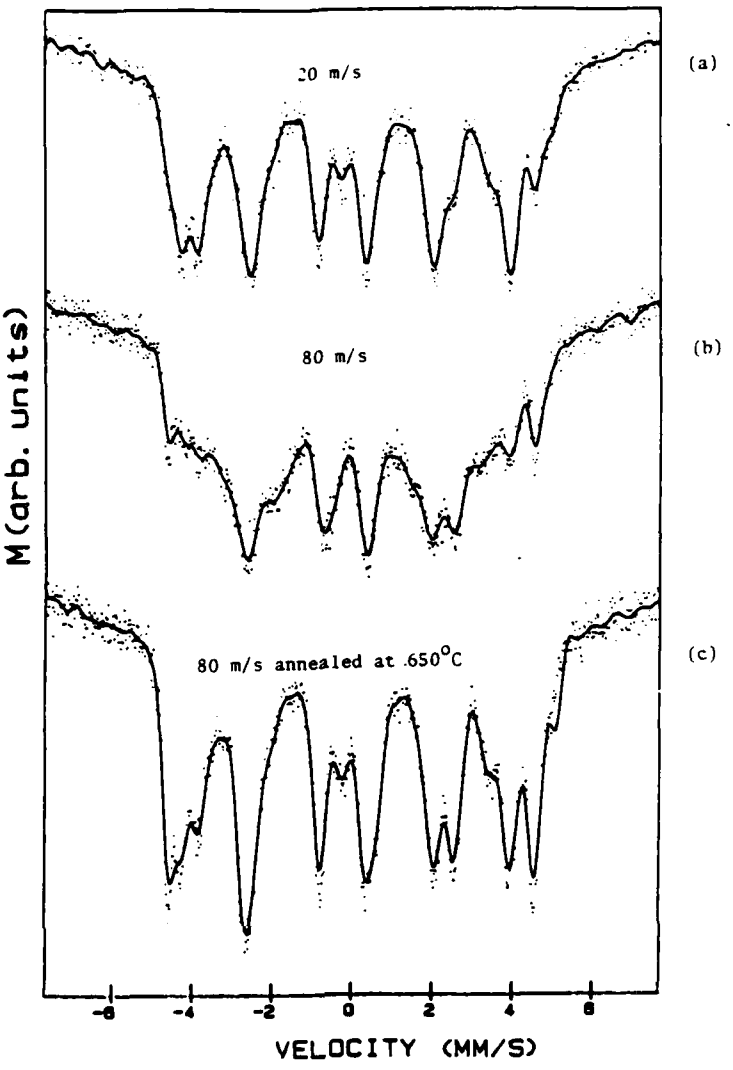

Figure 4-5. Mössbauer spectra for melt-spun $Fe_{76}Pr_{16}B_8$ (a) optimally quenched (20 m/s) (b) overquenched (80 m/s), and (c) overquenched and annealed at 650 °C for 25 minutes.

in the ribbon are specifically Nd_2Fe_{17} and $Fe_{14}Nd_2B$. However, the tetragonal phase is so complex that the spectrum of this phase mixed with most any soft ferromagnetic phase might look like Figure 4-8b. As stated before, the extreme complexity of the spectrum makes computer fitting extremely difficult at best. (One way to isolate the phases is to eliminate one ferromagnetic phase from the spectrum by heating above its Curie temperature while collecting the Mössbauer spectrum. This removes the magnetic hyperfine splitting and the phases can then be analyzed much more easily. This will be possible in the future at Vanderbilt as a result of the recent purchase of a ranger Scientific MS-900 Spectrometer and furnace.) At least one work[12] reports that these overquenched materials contain the tetragonal phase and a soft amorphous phase. Magnetization versus temperature curves indicate that the soft phase has a Curie temperature of about 160 °C.[1]

The spectrum for an underquenched ribbon (V_s = 6 m/s) (Figure 4-5b) appears to have peaks at the tetragonal positions. However, the peaks are poorly resolved even though the

Table 4-2
POSITION PARAMETERS FOR TETRAGONAL PHASE SITES

$Fe_{14}Nd_2B$

	ISOMER SHIFT	Hint.	QUAD. SPLITTING
K1 SITE			
PRESENT WORK	-.13	291	.18
REFERENCE 4	-.05	288	.25
REFERENCE 11	-.20	299	.03
K2 SITE			
PRESENT WORK	-.15	301	-.15
REFERENCE 4	-.10	307	.10
REFERENCE 11	-.02	286	.37
J1 SITE			
PRESENT WORK	.25	281	-.10
REFERENCE 4	-.17	264	.05
REFERENCE 11	.15	337	.74
J2 SITE			
PRESENT WORK	.03	339	.35
REFERENCE 4	.09	347	.60
REFERENCE 11	.05	294	.24
C OR E SITE			
PRESENT WORK	-.19	323	.27
REFERENCE 4	-.15	313	.24
REFERENCE 11	-.12	283	-.91
C OR E SITE			
PRESENT WORK	-.19	259	.06
REFERENCE 4	.09	263	.10
REFERENCE 11	-.06	261	.19
ADDITIONAL SITE			
PRESENT WORK	-.06	-	-
REFERENCE 4	.07	-	.69
REFERENCE 11	-	-	-

$Fe_{14}Pr_2B$

	ISOMER SHIFT	Hint.	QUAD. SPLITTING
K1 SITE			
PRESENT WORK	-.12	286	.16
REFERENCE 8	-.03+/-.04	282+/-4	.36
K2 SITE			
PRESENT WORK	-.18	306	-.26
REFERENCE 8	-.19	295	.03
J1 SITE			
PRESENT WORK	.28	286	-.11
REFERENCE 8	.04	291	.28
J2 SITE			
PRESENT WORK	.12	337	.25
REFERENCE 8	.08	336	.67
C OR E SITE			
PRESENT WORK	-.05	320	.21
REFERENCE 8	-.06	280	-.83
C OR E SITE			
PRESENT WORK	-.13	292	.06
REFERENCE 8	-.03	257	.24
ADDITIONAL SITE			
PRESENT WORK	.10	-	-
REFERENCE 8	-	-	-

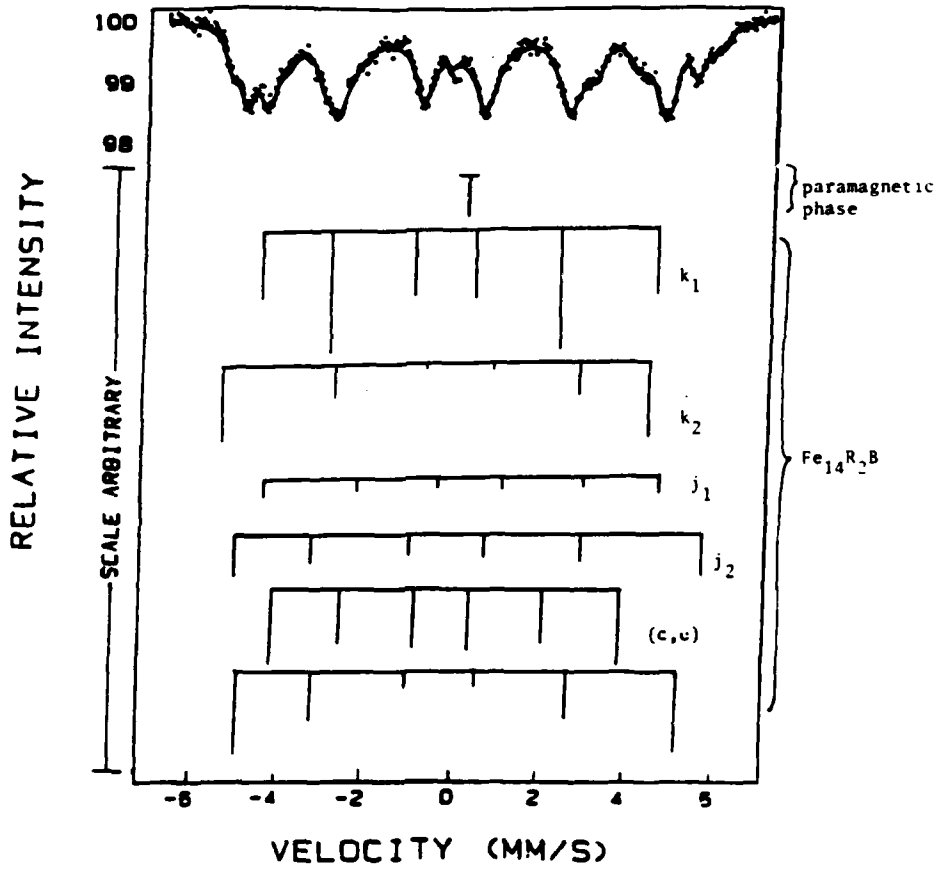

Figure 4-6. **Least square fit of an optimally quenched (20 m/s) $Fe_{76}Pr_{16}B_8$ Mössbauer spectrum. The bars represent the position and intensity of the various Fe lattice sites in the two phases assumed present.**

Table 4-3
HCI FOR PLASMA ARC MATERIALS

Plasma arc sprayed $Fe_{76}Pr_{16}B_8$

Same #		Hci
5		10.09
6		6.27
6	annealed at 350°C	9.03
6	annealed at 400°C	8.41
6	annealed at 400°C	7.94
6	annealed at 450°C	5.53
6	annealed at 500°C	4.53
6	annealed at 550°C	3.40

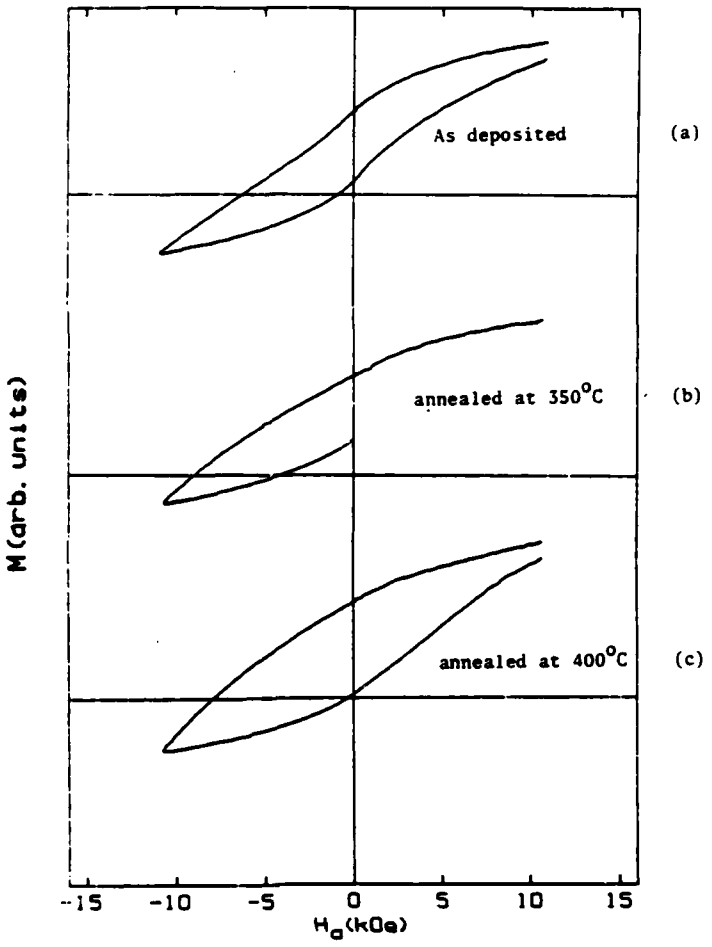

Figure 4-7. Hysteresis loops for plasma-spray deposited $Fe_{76}Nd_{16}B_8$ (a) before annealing (b) after annealing at 350 °C, for 25 minutes, and (c) after annealing at 400 °C for 25 minutes.

spectrum contains about the same number of background counts as the spectrum for the optimally quenched material. This lack of line intensity makes spectrum interpretation difficult.

Figure 4-3 contains Mössbauer spectra for an $Fe_{76}Nd_{16}B_8$ ingot and for melt-spun $Fe_{76}Nd_{16}B_8$ ribbons quenched at low, intermediate, and high values of V_s. The results are very much analogous to those found for the $Fe_{76}Pr_{16}b_8$ materials previously discussed (see Figure 4-1).

Annealing overquenched $Fe_{76}Pr_{16}B_8$ ribbons notably increases their magnetic coercivity, and this correlates with changes in the resultant Mössbauer spectra (see Figures 4-4 and 4-5). As shown in Table 4-1, annealing overquenched melt-spun ribbons at 650 °C for 25 minutes increased their intrinsic coercivity, Hc_i, from 1.34 kOe for V_s = 80 m/s. Hc_i for the sample quenched at the optimum wheel speed (V_s = 20 m/s) is 14.4 kOe. Figure 4-4 shows the changes in the Mössbauer spectra in going from an optimally quenched sample to an overquenched (60 m/s) sample to an annealed 60 m/s sample. As before, the spectrum of the optimally quenched sample indicates the presence of only the hard tetragonal phase and possibly a small amount of paramagnetic phase, while the spectrum of the overquenched sample

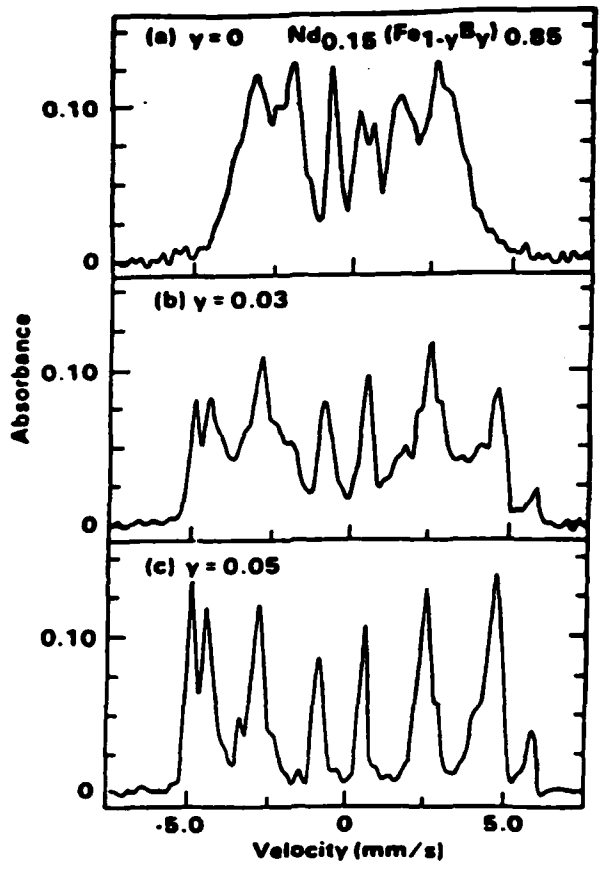

Figure 4-8. Mössbauer spectra for (a) $Fe_{17}Nd_2$ (b) a mixture of phases $Fe_{17}Nd_2$ and $Fe_{14}Nd_2B$, and (c) $Fe_{14}Nd_2B$.

(V_s = 60 m/s) appears to contain the tetragonal phase and a substantial amount of a soft ferromagnetic phase. In going from the optimally quenched spectrum to the overquenched spectrum, the peaks in the Doppler velocity range of −4 to −6 mm/s and +4 to +6 mm/s regions are strongly affected, indicating that the metastable phase produced by overquenching has peaks in these velocity ranges. Significantly, the spectrum of the annealed sample is very similar in appearance to the spectrum of the optimally quenched sample. The additional peaks showing up for the overquenched sample in the Doppler-velocity range from −4 to −6 mm/s and +4 to +6 mm/s disappeared, indicating that annealing caused the metastable, soft, second phase in the overquenched sample to transform into the stable tetragonal phase.

Figure 4-5 is the same as Figure 4-4 except that the overquenched sample was solidified at a wheel-surface speed of 80 m/s instead of 60 m/s. As expected, the Mössbauer spectrum (Figure 4-5b) is even more strongly disturbed over the same Doppler velocity ranges by the additional peaks. This increased disturbance is probably due to an increase in the fraction of the metastable phase relative to the tetragonal phase as the overquenching becomes more drastic. Annealing this sample increased the coercivity, but it was still considerably less than for the optimally quenched sample. The corresponding Mössbauer spectrum (Figure 4-5c) is still mixed-phase in appearance, but some of the soft phase present in the as-quenched material seems to have transformed into the tetragonal phase as a result of the anneal.

REFERENCES

1. Ruel Anthony Overfelt, "Rapidly Solidified Alloys of Iron-Rare Earth-Boron for Permanent Magnets," PhD Dissertation, Vanderbilt University, December 1984.
2. J.F. Herbst, J.J. Croat, and W.B. Yelon, *J. App. Phys. 57,* 4086 (1985).
3. J.J. Croat, J.F. Herbst, R.W. Lee, and F.E. Pinkerton, *J. App. Phys. 55,* 2087, (1984).
4. M. Sagawa, S. Fujimura, N. Togawa, H. Yamamoto, and Y. Matsurra, *J. App. Phys. 55,* 2083 (1984).
5. J.F. Herbst, J.J. Croat, F.E. Pinkerton, and W.B. Yelon *Phys. Rev. B, 29,* 4176 (1984).
6. J.D. Livingston, Proc. 8th Intl. Workshop on Rare-Earth Magnets, 423, May 1985.
7. Hideya Onodera, Yasoo Yamaguchi, H. Yamamoto, *J. Mag. and Mag. Matls. 46.* 151 (1984).
8. F.E. Pinkerton and W.R. Dunham, *J. App. Phys. 57,* 4121 (1985).
9. Richard L. Cohen "Elements of Mössbauer Spectroscopy," *Applications of Mössbauer Spectroscopy,* Vol. 1, pg. 16, Academic Press, NY (1976).
10. Ibid., pg. 24ff.
11. F.E. Pinkerton and W.R. Dunham, *App. Phys. Lett. 45,* 1248 (1984).
12. F.E. Pinkerton, private communication (July 1986).

Section 5

PUBLICATIONS, PRESENTATIONS, AND REPORTS

The review article "Iron Rare-Earth Permanent Magnets" by J.D. Livingston was presented in May 1985 at the 8th International Workshop on Rare-Earth Magnets in Dayton, Ohio, and published in the proceedings of that conference and as a General Electric CRD Report.

Other related lectures presented by J.D. Livingston include the following:

October 1985 - "Microstructure and Properties of Fe-Nd-B Magnets," AIME Fall Meeting, Toronto, Ontario, Canada.

November 1985 - "The New Super-Magnet: Fe-Nd-B," National Bureau of Standards, Gaithersburg, Maryland.

February 1986 - "Microstructure and Magnetic Properties," IEEE Section Meeting, Pittsburgh, Pennsylvania.

May 1986 - "New Frontiers in Magnetic Materials," MRS Regional Meeting, Rochester, New York.

June 1986 - "Coercivity in Rare Earth Magnets," 17th Rare Earth Research Conference, Hamilton, Ontario, Canada.

The article "Production of $Fe_{14}Nd_2B$ by a Reduction-Diffusion Process," by R. J. Zabala, J. D. Livingston, L. A. Johnson, and C. M. McFarland, has been published as a General Electric Report, 86CRD119.

END

10-86

DTIC